Glutathione transferases catalyze recycling of auto-toxic cyanogenic glucosides in sorghum

Nanna Bjarnholt*[1,2] (ID), Elizabeth H. J. Neilson[1,2], Christoph Crocoll[3], Kirsten Jørgensen[2], Mohammed Saddik Motawia[1,2], Carl Erik Olsen[1,2], David P. Dixon[4,†], Robert Edwards[4,‡] and Birger Lindberg Møller[1,2]

[1]*VILLUM Research Center for Plant Plasticity, Department of Plant and Environmental Sciences, University of Copenhagen, Frederiksberg 1871, Denmark,*
[2]*Plant Biochemistry Laboratory, Department of Plant and Environmental Sciences, University of Copenhagen, Frederiksberg 1871, Denmark,*
[3]*DynaMo Center, Department of Plant and Environmental Sciences, University of Copenhagen, Frederiksberg 1871, Denmark,*
[4]*Center for Bioactive Chemistry, Durham University, Durham DH1 3LE, UK,*

SUMMARY

Cyanogenic glucosides are nitrogen-containing specialized metabolites that provide chemical defense against herbivores and pathogens via the release of toxic hydrogen cyanide. It has been suggested that cyanogenic glucosides are also a store of nitrogen that can be remobilized for general metabolism via a previously unknown pathway. Here we reveal a recycling pathway for the cyanogenic glucoside dhurrin in sorghum (*Sorghum bicolor*) that avoids hydrogen cyanide formation. As demonstrated *in vitro*, the pathway proceeds via spontaneous formation of a dhurrin-derived glutathione conjugate, which undergoes reductive cleavage by glutathione transferases of the plant-specific lambda class (GSTLs) to produce *p*-hydroxyphenyl acetonitrile. This is further metabolized to *p*-hydroxyphenylacetic acid and free ammonia by nitrilases, and then glucosylated to form *p*-glucosyloxyphenylacetic acid. Two of the four GSTLs in sorghum exhibited high stereospecific catalytic activity towards the glutathione conjugate, and form a subclade in a phylogenetic tree of GSTLs in higher plants. The expression of the corresponding two *GSTLs* co-localized with expression of the genes encoding the *p*-hydroxyphenyl acetonitrile-metabolizing nitrilases at the cellular level. The elucidation of this pathway places GSTs as key players in a remarkable scheme for metabolic plasticity allowing plants to reverse the resource flow between general and specialized metabolism in actively growing tissue.

Keywords: nitrilases, cyanogenic glucosides, dhurrin, glutathione transferases, resource allocation, *Sorghum bicolor*.

INTRODUCTION

Plants produce a range of specialized metabolites to fend off herbivores and pests, to attract pollinators and adapt to a changing environment. One such class of compounds is comprised of the cyanogenic glycosides, which consist of an amino acid-derived carbon backbone and a cyanohydrin function stabilized through glucosylation. Cyanogenic glycosides are defense compounds widely distributed in terrestrial plants, including the pteridophytes, gymnosperms and angiosperms (Zagrobelny *et al.*, 2008). In many species these compounds are produced in very high concentrations. Prominent examples

are bitter almonds (*Prunus amygdalis*) and seeds of black cherry (*Prunus serotina*), tubers of cassava (*Manihot esculenta*) and the aerial tissues of eucalypts (*Eucalyptus* spp.), legumes and sorghum (*Sorghum bicolor*). In each case, cyanogenic glycosides comprise several percent of plant dry matter, thereby tying up an appreciable fraction of the plants' carbon and nitrogen pools (Swain and Poulton, 1994; Crush and Caradus, 1995; Gleadow and Woodrow, 2000; Busk and Møller, 2002; Forslund *et al.*, 2004; Jørgensen *et al.*, 2005; Sanchez-Perez *et al.*, 2008). In sorghum, biosynthesis of the cyanogenic glucoside dhurrin

(Figure 1) occurs rapidly in young seedlings and in developing grains and is in both cases accompanied by continuous further metabolism of the produced dhurrin. At later developmental stages, the rate of this metabolism exceeds that of biosynthesis, resulting in a net depletion of the total dhurrin pool (Adewusi, 1990; Busk and Møller, 2002; Nielsen *et al.*, 2016). Other cyanogenic species are also known to metabolize cyanogenic glycosides in the course of development. It has therefore often been suggested that in addition to their roles in defense, cyanogenic glycosides serve a dual purpose as storage compounds for reduced nitrogen that can be released for incorporation into general metabolites upon demand (Lieberei *et al.*, 1985; Swain and Poulton, 1994; Jørgensen *et al.*, 2005; Møller, 2010; Neilson *et al.*, 2011; Pičmanová *et al.*, 2015; Nielsen *et al.*, 2016). The mechanisms for cyanogenic glycoside recycling and N-remobilization have not been defined to date. However, recently, common types of likely derivatives of cyanogenic glycosides have been identified in three unrelated plant species, namely almond, cassava and sorghum. These plant species produce cyanogenic glycosides from four different amino acid precursors, pointing toward the existence of at least one conserved pathway (Pičmanová *et al.*, 2015; Blomstedt *et al.*, 2016).

The role of cyanogenic glycosides as defense compounds relies on their bioactivation by specific endogenous β-glucosidases (BGD) to release hydrogen cyanide (HCN), that is toxic to respiring organisms, including plants (Siegien and Bogatek, 2006). HCN is also formed as a by-product of ethylene biosynthesis in stoichiometric amounts (Peiser *et al.*, 1984). As such, all plants harbor an enzyme system for HCN detoxification and nitrogen recovery. Accordingly, it has been suggested that the recovery of nitrogen from stored cyanogenic glycosides proceeds *via* the bioactivation and detoxification pathways, outlined in Figure 1(a, b) (Miller and Conn, 1980; Swain and Poulton, 1994). In this pathway, β-cyanoalanine synthase (CAS) catalyzes the incorporation of the released HCN into β-cyanoalanine, which is then converted into asparagine and/or aspartate plus ammonia by members of the nitrilase 4 (NIT4) family. In most plants the reaction is catalyzed by a single NIT4 enzyme. However, grasses (Poaceae) possess two NIT4 homologs (NIT4A and NIT4B), with catalytic activity being dependent on heteromer formation between these isoforms (Figure 1b) (Jenrich *et al.*, 2007). In sorghum, three NIT4 isoforms (NIT4A, NIT4B1 and NIT4B2) are present, with the heteromer NIT4A/NITB2 able to hydrolyze *p*-hydroxyphenyl acetonitrile, as well as β-cyanoalanine (Figure 1c) (Jenrich *et al.*, 2007). Remarkably, the heteromer NIT4A/NITB1 was only found to hydrolyze β-cyanoalanine. Because of the structural resemblance of dhurrin and *p*-hydroxyphenyl acetonitrile, it was suggested that the NIT4A/NIT4B2 heterodimer is part of an uncharacterized pathway enabling recycling of nitrogen from dhurrin without releasing toxic HCN within plant cells (Jenrich *et al.*, 2007). In support of this hypothesis, expression of
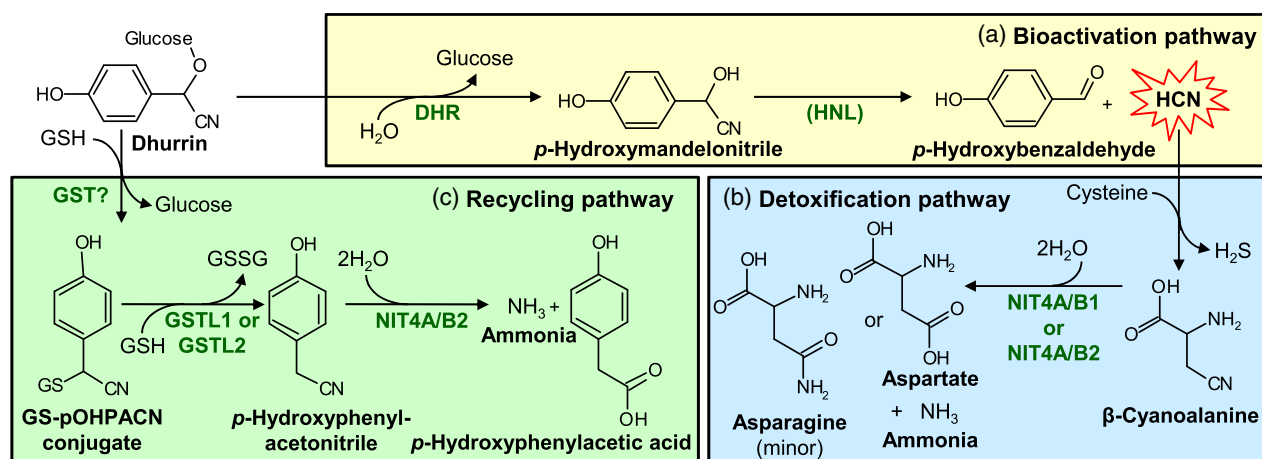

Figure 1. Bioactivation, detoxification and putative recycling pathway of the cyanogenic glucoside dhurrin in *Sorghum*.

(a) Dhurrin is hydrolyzed by a specific β-glucosidase, dhurrinase (DHR), forming an unstable cyanohydrin, *p*-hydroxymandelonitrile, which releases hydrogen cyanide (HCN), either spontaneously or mediated by the enzyme hydroxynitrile lyase (HNL).

(b) β-Cyanoalanine synthase (CAS) incorporates HCN into β-cyanoalanine that can be converted to asparagine, aspartate and ammonia by heteromers of nitrilases (NIT4) of the A and B types.

(c) Glutathione (GSH) replaces the glucose moiety in dhurrin, either spontaneously or mediated by an unknown glutathione transferase (GST). The resulting GS-conjugate of *p*-hydroxyphenyl acetonitrile (GS-pOHPACN, *p*-hydroxyphenyl(*S*-glutathione)acetonitrile) is cleaved by GSTs of the lambda class (GSTL) converting reduced GSH to its oxidized form (GSSG) and releasing *p*-hydroxyphenyl acetonitrile. This is the substrate for the sorghum NIT4 heteromer, which hydrolyses *p*-hydroxyphenyl acetonitrile to *p*-hydroxyphenylacetic acid and free ammonia, available for primary/general metabolism.

NIT4A/NIT4B2, but not of *NIT4B1*, was correlated with dhurrin depletion in the developing sorghum grain. In contrast, the two known β-glucosidases specific for the hydrolysis of dhurrin, dhurrinase 1 and 2, were not expressed (Nielsen *et al.*, 2016). As pointed out by Jenrich *et al.* (2007), the product of a putative pathway for dhurrin recycling proceeding via the hydrolysis of *p*-hydroxyphenyl acetonitrile catalyzed by the NIT4A/NIT4B2 heteromer would be *p*-hydroxyphenylacetic acid (Figure 1c). Previous studies have demonstrated the presence of the corresponding glucoside of this compound, namely *p*-glucosyloxyphenylacetic acid, in sorghum plants as well as in grains (Pičmanová *et al.*, 2015; Nielsen *et al.*, 2016). The accumulation of this conjugate was reduced to almost zero in *tcd2* sorghum mutant plants impaired in the last step of the dhurrin biosynthetic pathway (Blomstedt *et al.*, 2016). The evidence for a recycling pathway proceeding via non-BGD mediated conversion of dhurrin into *p*-hydroxyphenyl acetonitrile, *p*-hydroxyphenylacetic acid and subsequently *p*-glucosyloxyphenylacetic acid is therefore compelling. However, it has not been experimentally verified that the *p*-glucosyloxyphenylacetic acid found in sorghum is indeed derived from dhurrin and, if so, if and how dhurrin can be converted into *p*-hydroxyphenyl acetonitrile *in planta*. Here we address these issues and present evidence of the involvement of a specific class of glutathione transferase enzymes (GSTs) and their substrate, the tripeptide glutathione (GSH), in such a recycling pathway, as outlined in Figure 1(c).

RESULTS

Dhurrin accumulation and metabolism in young sorghum plants

To investigate the possible presence of a pathway for conversion of dhurrin to *p*-glucosyloxyphenylacetic acid, the total content of these two metabolites was quantified in young sorghum plants. In a representative experiment the dhurrin content decreased approximately 17 days after sowing, while the content of *p*-glucosyloxyphenylacetic acid increased throughout the experimental period (Figure 2). While the specific number of days that elapsed between sowing and maximal dhurrin content varied between experiments, in all cases the data confirmed that maximal dhurrin content was reached after day 10. Likewise, in all experiments, the replicates sampled around the time of maximal dhurrin content were subject to large variations, as seen in Figure 2, notably between days 13 and 24. Similar large variations in dhurrin content have been determined in developing sorghum grain (Nielsen *et al.*, 2016). This variation in dhurrin content indicates the onset of a change in the relative rates of synthesis vs. metabolism of dhurrin, with the differences between individual plants or grains giving rise to the variability. The total amount of *p*-glucosyloxyphenylacetic acid (abbreviated pGPAAc in figures) began to increase rapidly with plant age around the time at which the standard deviations on the measurements of dhurrin content indicated a change in overall metabolism (Figure 2). This is reflected
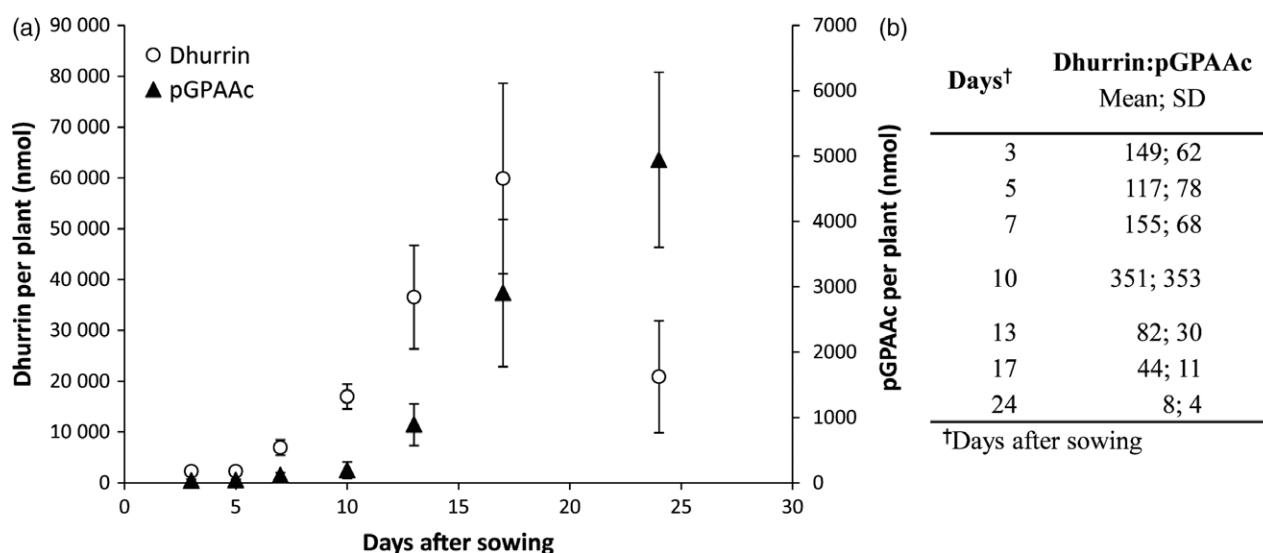

Figure 2. Content of dhurrin and *p*-glucosyloxyphenylacetic acid in *Sorghum* plants of increasing age.
pGPAAc = *p*-glucosyloxyphenylacetic acid. One biological replicate is the aerial tissue of a whole plant, including mesocotyl, node, coleoptile, sheaths and leaves. Each point is an average of three plants, except the last three points where 1–3 additional plants were analyzed to confirm that the large standard deviations were representative of the biological variation in the sample material.
(a) Total content of each compound plotted as function of plant age. Error bars represent standard deviations of biological replicates.
(b) The average of ratios between the two compounds in each replicate.

in the embedded table in Figure 2, showing the ratio dhurrin:*p*-glucosyloxyphenylacetic acid. This ratio was constant at the first three data points; at day 10 there was enormous variation and after that the ratio decreased, demonstrating that the rate of formation of *p*-glucosyloxy-phenylacetic acid exceeded that of dhurrin in the growth period covered by the last three data points. Neither free *p*-hydroxyphenylacetic acid, nor its suggested precursor *p*-hydroxyphenyl acetonitrile, were identified in the extracts.

To ascertain that *p*-glucosyloxyphenylacetic acid in sorghum is indeed derived from dhurrin, we carried out two different experiments. The first made use of the sorghum mutant line *tcd1* (*total cyanide deficient 1*). Plants of this line are mutated in the first enzyme of the dhurrin biosynthetic pathway (Blomstedt *et al.*, 2012), only accumulating minute amounts of dhurrin and no detectable *p*-glucosyloxyphenylacetic acid (Figure 3a). When a dhurrin solution was administered to excised *tcd1* leaves an appreciable amount of *p*-glucosyloxyphenylacetic acid was accumulated, verifying their metabolic relationship (Figure 3a, similar data for leaves from older plants are provided in Figure S1). In the second experiment, intact wildtype plants were administered ^{14}C-labeled L-tyrosine at the 2½ leaf stage (5 days old) and the plants harvested 3, 6 and 11 days after uptake. An initial experiment showed that at all time points, the majority of radiolabel was found in the node and in the leaves that were developed at the time of administration. Leaf 2 was fully developed at 5 days and remained green throughout the experiment. From each plant, leaf 2 was therefore harvested, extracted and analyzed separately, and also analyzed in combination with extracts of the remaining plant tissues (respectively 'leaf 2' and 'total plant' in Figures 3b, c and Figure S2). The total incorporation of label into dhurrin was relatively uniform between replicates (Figures 3c and S2), but decreased over the course of the experiment, demonstrating the continuous metabolism of dhurrin. In the TLC analysis of total plant extracts, the radiolabeled spots pertaining from *p*-glucosyloxyphenylacetic acid were increasing in intensity with time, although at levels too weak to be reliably quantified (Figure S2). In leaf 2 extracts it was possible to quantify the intensity of ^{14}C-labeled *p*-glucosyloxyphenylacetic acid spots, and it was found to increase by approximately 130% from 3 to 11 days after uptake, while the ratio ^{14}C-dhurrin : [14]C-*p*-glucosyloxyphenylacetic acid decreased by a factor 3 (Figure 3c). Remarkably, total ^{14}C in total extracts also decreased over time, demonstrating loss of label to either roots, atmosphere or the insoluble fraction. In the soluble fraction, only very few other compounds than dhurrin and *p*-glucosyloxyphenylacetic acid were found to be labelled (Figure S2), and none of them co-eluted with known compounds.
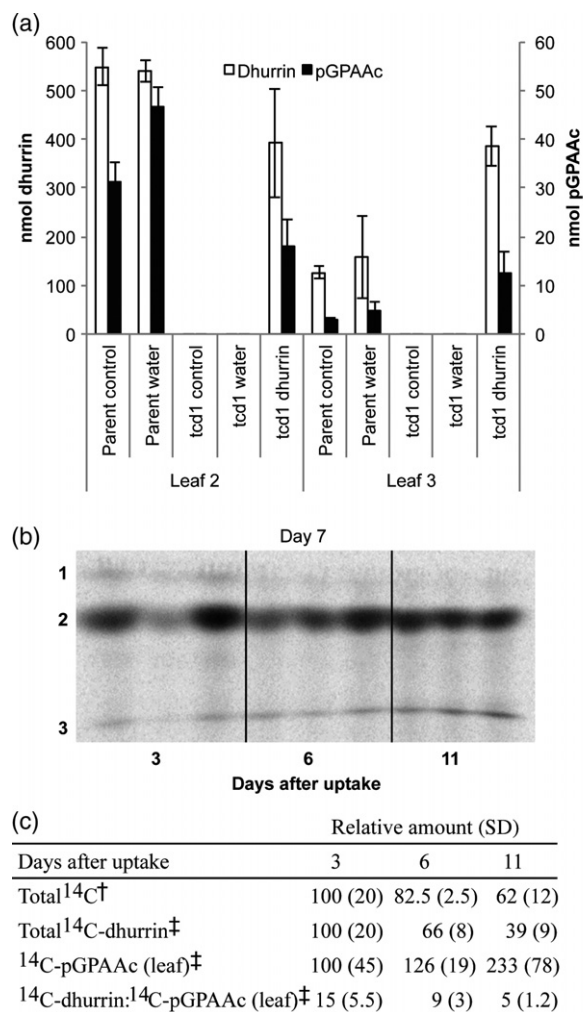

(a)

(b) Day 7

(c)

Days after uptake	Relative amount (SD)		
	3	6	11
Total [14]C[†]	100 (20)	82.5 (2.5)	62 (12)
Total ^{14}C-dhurrin[‡]	100 (20)	66 (8)	39 (9)
[14]C-pGPAAc (leaf)[‡]	100 (45)	126 (19)	233 (78)
[14]C-dhurrin:[14]C-pGPAAc (leaf)[‡]	15 (5.5)	9 (3)	5 (1.2)

[†]Determined in total plant extracts by scintillation counting
[‡]Determined by spot quantification in TLC analyses of respectively total plant extracts (Figure S2) and leaf 2 extracts (leaf) (panel B).

Figure 3. *In planta* production of *p*-glucosyloxyphenylacetic acid from dhurrin.
(a) The second- and third-oldest leaves from 7 days old plants were excised below the blade and administered either 500 nmol dhurrin in 50 µl water ('dhurrin') or the same volume of water ('water') by uptake through the cut. After uptake, the leaves were incubated for 5 h and then snap frozen. 'Control' leaves were harvested directly into liquid nitrogen at t = 0. 'Parent' = parent line, '*tcd1*' = 'total cyanide deficient' mutant line. Error bars represent standard deviations of biological replicates, *n* = 3.
(b) Production of ^{14}C-labelled dhurrin and *p*-glucosyloxyphenylacetic acid in WT plants following administration of ^{14}C-tyrosine to intact plants. The results were analyzed by TLC, here shown for extracts of leaf 2 (TLC analysis of total plant extracts in Figure S2). 1 = *p*-hydroxybenzaldehyde, 2 = dhurrin, 3 = *p*-glucosyloxyphenylacetic acid.
(c) Quantification of ^{14}C in relevant fractions from the experiment described in (b).

Identification of GSH conjugation products of dhurrin

When investigating nitrilase activity *in vitro*, a reductant is often added to the assay mixture to stabilize enzyme activity (Jenrich *et al.*, 2007). In previous studies (Jenrich *et al.*, 2007), the classical reductant dithiothreitol (DTT) was

found to cause a chemical conversion of dhurrin into *p*-hydroxyphenyl acetonitrile. On testing other reductants, we found that β-mercaptoethanol caused the same chemical conversion as DTT, while the tripeptide glutathione (GSH), a ubiquitous antioxidant in plants, undergoes different chemical reactions with dhurrin. As determined by LC-MS/MS analysis of samples containing dhurrin incubated with GSH, the reaction products resulted in two peaks of *m/z* 439 (Figure S3), with this ion producing a major fragment at *m/z* 310 and a minor entity at *m/z* 364. Such neutral losses of respectively 129 or 75 Da are commonly observed in positive mode electrospray when analyzing GS-conjugates by LC-MS/MS (Chen *et al.*, 2008; Xie *et al.*, 2013). The compounds were produced *in vitro*, purified by preparative HPLC and their structures elucidated by NMR (see the Experimental Procedures section, Figure S3 and Table S1 for chemical shifts and their assignments). It was determined that GSH had substituted the glucose in dhurrin to form glutathionylated *p*-hydroxyphenyl acetonitrile (GS-pOHPACN, Figure 1c). As determined by LC-MS/MS and NMR, the *in vitro* reaction produced a ~50:50 mixture of GS-pOHPACN epimers, indicating that the conjugate formation proceeded by a S_N1 nucleophilic substitution reaction. The two epimers were named GS-pOHPACN 1 and GS-pOHPACN 2, reflecting their order of elution from the HPLC column. No attempts were made to clarify the configuration around the dhurrin-derived chiral carbon. GS-pOHPACN formation was inhibited at pH < 5 and promoted with increasing pH. This is consistent with the previous finding that dhurrin forms a reactive quinone tautomer at high pH, which in the absence of other reactants causes hydrolysis of the *O*-glucosidic bond and the non-enzymatic formation of HCN and *p*-hydroxybenzaldehyde (Mao and Anderson, 1965; Møller *et al.*, 2016). The GS-pOHPACN epimers isomerized rapidly at pH > 5. When one epimer was incubated at pH 7.5 (30°C), 5% isomerized into the other within 1 min. After a 30 min incubation, an equilibrium was reached, resulting in a ~50:50 mixture of GS-pOHPACN epimers.

Having identified this GSH-mediated reaction *in vitro*, the sorghum plant extracts (Figure 2) were re-analyzed to determine if these characteristic conjugates could be detected *in vivo*. GS-pOHPACN was present in small amounts in the extracts, but only detectable in all replicates at days 3 (trace), 7 (9 nmol/plant, s.d. 3 nmol/plant) and 24 (190 nmol/plant, s.d. 163 nmol/plant). The measured concentrations were adequate to allow quantification, but not to determine which of the GS-pOHPACN epimers were present *in planta*. Upon revisiting the metabolite analyses data of earlier studies (Nielsen *et al.*, 2016), the conjugate was also detected in small amounts at the end of sorghum grain development, when dhurrin content was rapidly declining (Figure S4).

Dhurrin metabolizing enzyme activities in sorghum seedlings

The discovery of GS-pOHPACN prompted us to investigate whether GSTs were involved in dhurrin recycling. GSTs are known to catalyze a range of conjugation and reductive reactions using GSH as a co-substrate or co-factor (Dixon and Edwards, 2010a; Cummins *et al.*, 2011; Labrou *et al.*, 2015). Soluble protein was extracted from the same batch of sorghum plants as used for the metabolite analysis (Figure 2) and assayed for relevant GST and nitrilase activities. When the plant protein extracts were supplied with GS-pOHPACN 2 as substrate, in the presence of GSH, *p*-hydroxyphenyl acetonitrile and *p*-hydroxyphenylacetic acid were produced in the samples (Figure 4b). In the absence of plant extract, no products were detected and no substrate was consumed. Likewise, incubation with GS-pOHPACN 1 did not give rise to any detectable product formation or substrate consumption (Figure 4a). The incubation time was kept at 5 min to minimize isomerization, and the results therefore demonstrate specific conversion of a single GS-pOHPACN epimer, pointing towards an enzyme catalyzed reaction.

The plant protein extracts were also incubated with dhurrin in the presence of GSH, giving rise to the production of GS-pOHPACN as well as *p*-hydroxyphenyl acetonitrile and *p*-hydroxyphenylacetic acid (Figure 4c). The dominant product was *p*-hydroxybenzaldehyde formed from the highly active bioactivation pathway (Figure 4d). This overwhelming dhurrinase activity rapidly consumed the supplemented dhurrin, and it was therefore necessary to use a high concentration of substrate (2.5 mM) and extend the incubation time (45 min) to detect the putative recycling pathway products. This explains why in these samples trace amounts of *p*-hydroxyphenylacetamide were also detected, as this compound is a minor by-product of the nitrilases from sorghum formed *in vitro* (Agerbirk *et al.*, 2008). Under these prolonged assay conditions, in the absence of plant extract, the only product was GS-pOHPACN (Figure 4d), further supporting that conversion of GS-pOHPACN to *p*-hydroxyphenyl acetonitrile was not due to a spontaneous chemical reaction. The combined amount of GS-pOHPACN, *p*-hydroxyphenyl acetonitrile and *p*-hydroxyphenylacetic acid produced, was much less than the amount of GS-pOHPACN formed in the protein-free control incubations. It was concluded that the high dhurrinase activity present in the extracts prevented the detection of possible enzyme catalyzed formation of GS-pOHPACN from dhurrin. Significantly, the highest levels of GS-pOHPACN determined in the enzyme assays were with protein extracts from those plants in which the compound was also found in quantifiable amounts in the metabolite extracts, namely day 7 and day 24 (Figure 4). This indicated that the higher level of GS-pOHPACN found in plants
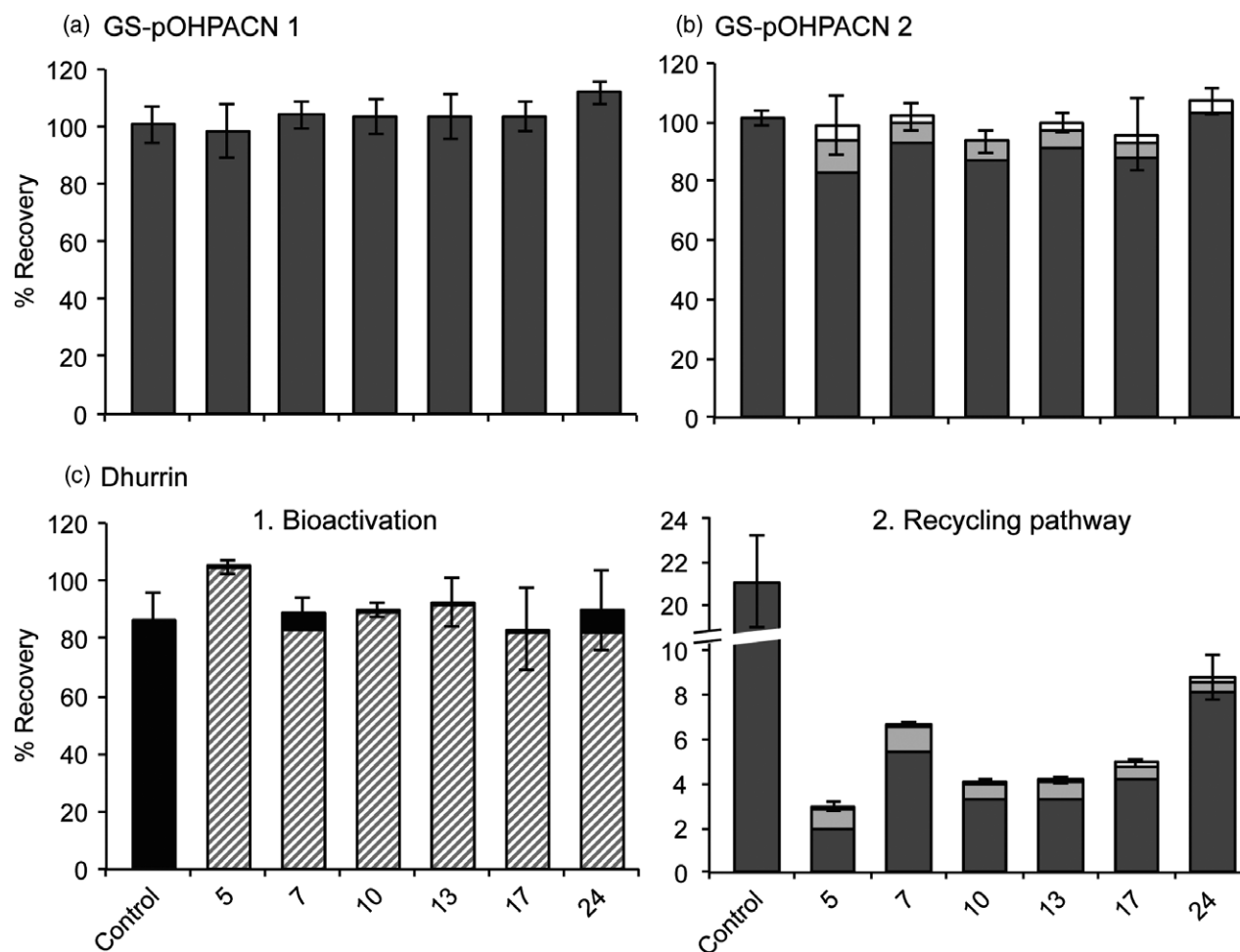
Figure 4. Dhurrin metabolizing enzyme activities in sorghum plants.

Soluble protein was extracted from plants of increasing age (x-axes, 5, 7, 10, 13, 17, 24 days after sowing) and incubated with different substrates from the proposed pathway for dhurrin turnover.

(a) Substrate = 0.2 mM GS-pOHPACN 1, incubation = 5 min.

(b) Substrate = 0.2 mM GS-pOHPACN 2, incubation = 5 min.

(c) Substrate = 2.5 mM dhurrin, incubation = 45 min. Due to order of magnitude difference in recovery of different products the results have been split into c1: Substrate recovery (dhurrin) and bioactivation pathway (p-hydroxybenzaldehyde), and c2: Recycling pathway products. Note the different scale and hatched y-axis.

Detected products across all charts: dark grey = GS-pOHPACN, light grey = *p*-hydroxyphenylacetonitrile, white = *p*-hydroxyphenylacetic acid, black = dhurrin, hatched bars = *p*-hydroxybenzaldehyde. In all charts the products are presented as % recovery of added substrate; in the control the substrate was incubated in assay buffer without protein. All experiments were performed in triplicate (technical replicates), and error bars represent standard deviations of the sum of quantified products.

at these two time points was defined by components of the soluble protein fraction.

Novel roles for GSTs in dhurrin recycling

The dhurrin derivatives formed in the plant protein extracts in the presence of GSH revealed the existence of a protein component with the ability to catalyze the reductive cleavage of GS-pOHPACN. Orthologous GSH-dependent activities have previously been determined with members of plant specific subclasses of the GST enzyme superfamily (GSTs, EC 2.5.1.18), notably the dehydroascorbate reductases (DHARs) and the lambda GSTs (GSTLs) (Dixon *et al.*, 2002; Dixon and Edwards, 2010b; Lallement *et al.*, 2014b). Thus these enzymes are known to catalyze the reductive cleavage of GSH conjugates, resulting in removal of GSH from the molecules (see GSTL reaction; Figure 1c). In the sorghum genome (http://phytozome.jgi.doe.gov/pz/portal.html#), three sequences for putative *Sb*DHAR enzymes and four putative *Sb*GSTLs have been identified based on *in silico* analysis of GSTs from all published plant genomes (Lallement *et al.*, 2014b). Furthermore, the expression of these genes has been confirmed by transcriptomics in developing sorghum grain (Nielsen *et al.*, 2016). To examine their function, synthetic genes encoding all seven

putative GSTs were expressed in *Escherichia coli* (*E. coli*) and the resulting proteins tested for their ability to metabolize dhurrin and GS-pOHPACN. Only the members of the GSTL class were found to exert activity on these substrates, and as such were selected for further analyses.

The *GSTL*s were cloned from sorghum cDNA to verify that the expressed coding sequences corresponded to those derived from the genomic sequences and transcriptomics experiment. The corresponding enzymes were named *Sb*GSTL1 to *Sb*GSTL4, respectively, and the genes encoding them termed *SbGSTL1* (transcript Sobic.002G4 21200.2), *SbGSTL2* (transcript Sobic.009G033200.2), *SbGSTL3* (transcript Sobic.001G412700.1) and *SbGSTL4* (transcript Sobic.001G412800.2). Of these, *Sb*GSTL1 and *Sb*GSTL2 were 94% identical and shared low identity with the other GSTLs (32–51%) (Figure S4 and Data S1). A phylogenetic analysis of GSTLs from sorghum, wheat, rice, Arabidopsis, poplar and maize identified that *Sb*GSTL1 and *Sb*GSTL2 form a specific subgroup (Figure 5). This suggested that they had evolved into a sub-clade early after the emergence of lambda GSTs. In contrast, *Sb*GSTL3 and *Sb*GSTL4 shared more than 65% identity with other monocot GSTLs and are apparently members of two different GSTL subgroups. *Sb*GSTL4 had a predicted chloroplast targeting peptide (aa 1–15). Plastid targeted GSTLs have been identified in other plants, e.g. in Arabidopsis
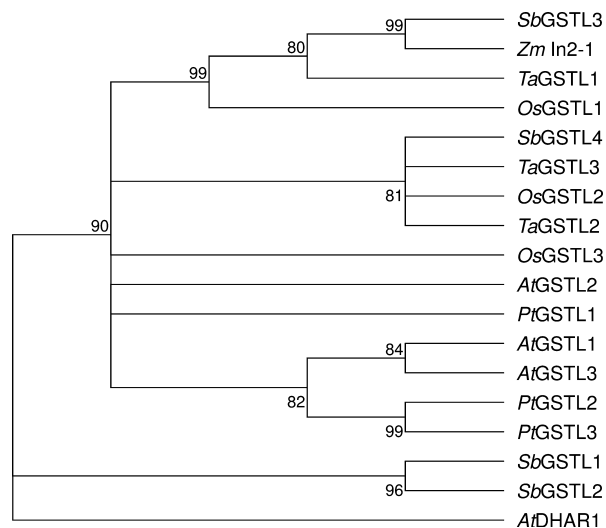
[*At*GSTL2 (Dixon *et al.*, 2002)] and poplar [*Pt*GSTL1 (Lallement *et al.*, 2014b)].

The coding sequences of the four *GSTL* genes and that of a truncated version of *SbGSTL4* lacking the chloroplast targeting peptide were expressed in *E. coli* with an N-terminal Strep3-tag and purified. The recombinant enzyme preparations were then tested for their ability to catalyze the GS-pOHPACN cleavage reaction. The experiments were also carried out using dhurrin and the reference compound 4NPG (*S*-(4-nitrophenacyl)glutathione) as substrates. For comparison with the enzymes from sorghum, purified Strep3-tagged GSTLs from *Arabidopsis* (Dixon *et al.*, 2009) and wheat (Dixon and Edwards, 2010b) were also assayed at a fixed, high concentration of GS-pOHPACN (500 μM). The reaction's pH dependency was determined for *Sb*GSTL2 using GS-pOHPACN 2 as substrate. While the reaction rate was similar at pH 6–6.5, it was found to increase between pH 6.5–8. Most plant GSTs, including all lambda GSTs investigated to date, have been found to be soluble enzymes. Furthermore, in localization experiments the majority of GSTs have been found to be cytosolic, with a few exceptions mainly ascribed to predicted target peptides on the enzymes (Dixon *et al.*, 2002, 2009; Lan *et al.*, 2009; Dixon and Edwards, 2010b; Liu *et al.*, 2013; Lallement *et al.*, 2014b). Here, only one enzyme had a predicted target peptide (*Sb*GSTL4), and therefore the remaining experiments were carried out at pH 7.5 to ensure near optimal conditions for the enzyme activity while remaining at a realistic pH for a cytosolic reaction. The GSTL catalyzed reductive cleavage reaction rate depends on the binding of the co-factor GSH, along with the conjugate molecule. To monitor specifically the affinity of the GSTL enzymes for the conjugate molecule, the assays were performed in the presence of a large excess of GSH. To minimize the effects of GS-pOHPACN isomerization, incubation times were minimized and the isomerization reaction excluded from the calculations of the kinetic parameters. The resulting apparent K_m and k_{cat} values with respect to the two different GS-pOHPACN epimers are presented in Table 1.

Of the 11 different GSTL enzymes tested for their ability to convert GS-pOHPACN to *p*-hydroxyphenyl acetonitrile, nine were found to be active (Tables 1 and S2). *Sb*GSTL3 and *Ta*GSTL1 were not able to metabolize GS-pOHPACN. While the three catalytically active *Sb*GSTLs had K_m values in the same range, the catalytic efficiencies (k_{cat}/K_m) for *Sb*GSTL1 and *Sb*GSTL2 were 10–100-fold higher than for *Sb*GSTL4 and Δ*Sb*GSTL4. The turnover numbers determined for wheat and *Arabidopsis* GSTLs at high substrate concentrations were also low compared with k_{cat} values for *Sb*GSTL1 and *Sb*GSTL2. Importantly, *Sb*GSTL1 and *Sb*GSTL2 were the only two enzymes demonstrating clear preference for a specific GS-pOHPACN epimer, namely GS-pOHPACN 2, as also determined in the sorghum plant protein extracts (Figure 4a, b). The compound 4-NPG is

Figure 5. Maximum likelihood phylogenetic tree of GSTLs from different plants.
Sequences from other plants than sorghum: *Arabidopsis thaliana*, *At*GSTL1-*At*GSTL3 (Dixon *et al.*, 2002, 2009), wheat (*Triticum aestivum*), *Ta*GSTL1-*Ta*GSTL3 (Dixon and Edwards, 2010b), rice (*Oryza sativa*) *Os*GSTL1-*Os*GSTL3 (Kumar *et al.*, 2013), maize (*Zea mays*), *Zm* In2–1 (Hershey and Stoner, 1991), poplar (*Populus trichocarpa*), *Pt*GSTL1-*Pt*GSTL3 (Lan *et al.*, 2009). Bootstrap = 1000. Condensed branch lengths were computed with 70 as the cut-off value. Due to significant deviations at the ends of some of the proteins *Sb*GSTL4, *Os*GSTL3 and *Pt*GSTL1-*Pt*GSTL3 (Lallement *et al.*, 2014b)) from the remaining sequences, another tree was constructed in which the ends were trimmed and the sequences realigned. The result was the same.

Table 1 Kinetic parameters determined for GSTL enzymes from sorghum compared to other plants

	Kinetic parameters					
	k_{cat} (min^{-1} ± SEM)* GS-pOHPACN[†]		K_m (µM ± SEM)* GS-pOHPACN		k_{cat}/K_m (min^{-1} µM^{-1} ± SEM) GS-pOHPACN	
Enzyme	1	2	1	2	1	2
*Sb*GSTL1	203 ± 12	674 ± 37	30 ± 5	25 ± 4	7 ± 1	28 ± 5
*Sb*GSTL2	143 ± 8	290 ± 21	4 ± 1	4 ± 1	40 ± 9	73 ± 25
*Sb*GSTL3	n.a.[‡]					
*Sb*GSTL4	n.d.[§]	14 ± 1	n.d.	10 ± 2		1 ± 0.3
*Sb*ΔGSTL4	8 ± 0.4	7 ± 0.3	15 ± 2	10 ± 2	0.6 ± 0.1	0.7 ± 0.1

	Turnover number[¶] (min^{-1}; SD) GS-pOHPACN	
Enzyme	1	2
*Ta*GSTL1	n.a.	n.a.
*Ta*GSTL3	56; 7	64; 6
*At*GSTL3	15; 0.3	14; 0.5

*Results for k_{cat} and K_m are means of three experimental replicates.
[†]GS-pOHPACN 1 and 2 refer to the earlier and later eluting epimer, respectively.
[‡]n.a. = no activity.
[§]n.d. = not determined (due to low yield of purified *Sb*GSTL4, k_{cat} and K_m were only determined for GS-pOHPACN 2).
[¶]Due to limited substrate availability, *Ta* and *At* enzymes were assayed at one fixed concentration, and only the two most active and the completely inactive *Ta*GSTL1 were assayed in duplicate, with the means of the resulting turnover numbers shown here. Single measurements of the activity of the remaining *Ta* and *At* enzymes are found in Table S2.

structurally similar to GS-pOHPACN and was previously identified as a substrate for the human GST, omega GST 1–1, which also carries out reductive cleavage reactions (Board *et al.*, 2008). In the present study, the activity towards 4-NPG was used to verify that the recombinant *Sb*GSTL3 was catalytically active and to further substantiate that GS-pOHPACN is likely to be a physiological substrate of *Sb*GSTL1 and *Sb*GSTL2. Using 4-NPG as substrate for *Sb*GSTL1 and *Sb*GSTL2, V_{max} was not reached even at a substrate concentration of 500 µM, indicating that the K_m for 4-NPG was much higher than for both of the GS-pOHPACN epimers. The turnover numbers were respectively 466 min^{-1} (s.d. 13 min^{-1}) and 402 min^{-1} (s.d. 94 min^{-1}) at this substrate concentration. *Sb*GSTL3 and *Sb*ΔGSTL4 both displayed relatively high K_m (33 µM (s.d. 18 µM) and 54 µM (s.d. 31 µM), respectively) and relatively low catalytic efficiencies [both 2 min^{-1} µM^{-1} (s.d. 1 min^{-1} µM^{-1})] with 4-NPG as substrate.

In the bacterium *Sphingomonas chlorophenolica*, GSTs catalyze the reductive cleavage of pentachlorophenol, in a two-step dechlorination reaction. In the first step, a chlorine atom is replaced by GSH, which is then subsequently removed in a reductive cleavage reaction (McCarthy *et al.*, 1996; Huang *et al.*, 2008). Consequently, these GSTs are both glutathionylating and de-glutathionylating enzymes. Dhurrin was therefore tested as a substrate for the *Sb*GSTLs in the presence of GSH to determine whether GS-pOHPACN is an intermediate in a single enzyme catalyzed conversion of dhurrin to *p*-hydroxyphenyl acetonitrile. When the *Sb*GSTLs were supplied with dhurrin, no *p*-hydroxyphenyl acetonitrile-forming activity could be detected during the short term incubations giving rise to the data in Table 1, demonstrating that dhurrin was not a substrate. Formation of *p*-hydroxyphenyl acetonitrile was detected following prolonged incubation due to the chemical conversion of dhurrin to GS-pOHPACN. The *Sb*GSTLs were also assayed in combination with each other to test the possibility that heteromer formation is essential for their catalytic activity, as observed for the sorghum NIT4 nitrilases (Jenrich *et al.*, 2007). When the enzymes were tested in combination, the total *p*-hydroxyphenyl acetonitrile-forming activity was equal to the sum of the activities of the individual enzymes.

Site of expression of the genes involved in the recycling pathway

In situ PCR experiments (Koltai and Bird, 2000; Jørgensen *et al.*, 2005, 2011) were carried out to investigate in which cell types the sorghum *GSTL*s and *NIT4*s were expressed. Experiments were performed using sorghum plants grown for 7 and 10 days. At these time points, enzymes involved in dhurrin recycling would be expected to be active and increasing in amount (Figures 2 and 4), with the corresponding transcripts therefore likely to be present. Figure 6 presents images from two different representative experiments (supported by additional images in Figures S6 and S7). Images in Figure 6(1a–1d) display when and where the GS-pOHPACN metabolizing *GSTL*s were expressed, and images in Figure 6(2a–2d) visualize *NIT4* gene expression compared to *Sb*GSTL1. Expression of mRNAs encoding

SbGSTL1 or *SbGSTL2* in the third leaf from 10-day-old plants was always found exclusively in the sheath bundle cells and in parenchyma cells surrounding the vascular bundle (Figure 6,1a, 1b). In contrast, *SbGSTL4* expression as observed in the leaf of a 7-day-old plant was more dispersed, with the respective mRNA found in the epidermis and cortex as well as scattered in parenchyma cells around the vascular bundles (Figure 6,1c). Importantly, the *SbGSTL4* transcript was not detectable at day 10 whereas *SbGSTL1* was detected both at day 7 and 10, in the same cells (Figure S6). The nitrilases *SbNIT4A* (Figure 6,2b) and *SbNIT4B2* (Figure 6,2d) were consistently found to be expressed in the same cells as *SbGSTL1* (Figure 6,2a). In contrast, mRNA from the nitrilase *SbNIT4B1*, which is not involved in conversion of *p*-hydroxyphenyl acetonitrile to *p*-hydroxyphenylacetic acid, could not be detected (Figure 6,2c).

DISCUSSION

In this study we have elucidated an endogenous pathway for recycling of the cyanogenic glucoside dhurrin in sorghum. The pathway proceeds via the intermediates GS-pOHPACN, *p*-hydroxyphenyl acetonitrile and *p*-hydroxyphenylacetic with concomitant release of ammonia (Jenrich *et al.*, 2007) and presumably glucose. The identification of the minimal set of genes and enzymes enabling recovery of nitrogen from dhurrin in sorghum finally corroborates the hypothesis that the defense compounds cyanogenic glycosides serve additional roles as storage compounds for reduced nitrogen.

Endogenous metabolism of dhurrin in sorghum was previously observed (Adewusi, 1990; Busk and Møller, 2002; Nielsen *et al.*, 2016) and was proposed to involve the action of the *Sb*NIT4A/NIT4B2 heteromer that catalyzed conversion of *p*-hydroxyphenyl acetonitrile into *p*-hydroxyphenylacetic acid (Jenrich *et al.*, 2007). In the GSH-dependent pathway identified here, the conversion of dhurrin to the *Sb*NIT4A/NIT4B2 substrate is predicated on dhurrin first reacting non-enzymatically with GSH to form a conjugate that then undergoes reductive cleavage catalyzed by a GSTL. In the plant cytosol, the GSH concentration has been reported to be 0.2–3 mM (Meyer *et al.*, 2001; Hartmann *et al.*, 2003), making it readily available for participation in metabolic processes. Although GSH is normally thought to be involved in the detoxification of xenobiotics and in maintaining redox balance, it is also known to be a building block in biosynthesis of specialized metabolites (Geu-Flores *et al.*, 2009, 2011; Kobayashi *et al.*, 2011; Su *et al.*, 2011; Fedrizzi *et al.*, 2012). Molecules conjugated with GSH are rarely detected in plants, but have for example been shown to be intermediates in the biosynthesis of glucosinolates and camalexin. The involved GS-conjugates were only accumulated and detected when the biosynthetic pathways were truncated (Geu-Flores *et al.*, 2009, 2011),

confirming that their formation is transient. In the current study, small amounts of GS-pOHPACN were only detected at very specific time points although dhurrin metabolism took place at all time points studied (Figures 2 and 4). A similar situation was observed in the developing sorghum grain (Figure S4) (Nielsen *et al.*, 2016).

The involvement of GSTs in dhurrin metabolism adds new insight into the multiple functions of these enzymes *in planta*. GSTs are diverse and highly abundant in cereals, typically encoded by between 50–80 genes in higher plants (Dixon and Edwards, 2010a; Jain *et al.*, 2010; Chi *et al.*, 2011; Rezaei *et al.*, 2013). Plant GSTs are divided into 14–15 classes, of which six are plant specific, a few are only present in early plant lineages, and one is an evolutionarily distinct microsomal class of membrane bound enzymes conserved across kingdoms (Jain *et al.*, 2010; Cummins *et al.*, 2011; Liu *et al.*, 2013; Lallement *et al.*, 2014a). Despite the abundance and diversity of plant GSTs and many reports about their *in vitro* activities and role in herbicide detoxification, knowledge about their *in vivo* functions and physiological roles is scarce (Dixon *et al.*, 2010; Cummins *et al.*, 2011; Labrou *et al.*, 2015). Classical GST enzymes catalyze a glutathionylation reaction proceeding via the nucleophilic attack of the thiol group of glutathione (GSH). Across all kingdoms, GST classes exist in which the classical catalytic residue (typically serine in plants) has been replaced by a cysteine (Cys-GSTs), generally rendering the enzymes unable to catalyze glutathionylation reactions (Dixon *et al.*, 2002; Board *et al.*, 2008; Xun *et al.*, 2010; Lallement *et al.*, 2014a,b). In plants, DHARs and GSTLs are such Cys-GSTs. While they do not catalyze the conjugation of xenobiotics with GSH they do have roles in redox homeostasis. For example the DHARs function in the recycling of ascorbate (DHAR = DeHydroAscorbate Reductase) (Urano *et al.*, 2000; Dixon *et al.*, 2002) and/or GSH (Rahantaniaina *et al.*, 2017). In contrast, no specific *in vivo* function has previously been assigned to GSTLs. Likewise, cleavage of GS-conjugates has not previously been demonstrated as a GST catalyzed reaction operating *in planta*. It was therefore surprising to discover sorghum GSTLs committed to deglutathionylation of GS-pOHPACN to *p*-hydroxyphenyl acetonitrile in endogenous plant metabolism. GSTLs from wheat, *Arabidopsis* and poplar as well as other Cys-GSTs from mammals and microbes catalyze the reductive cleavage of aromatic GSH conjugates (McCarthy *et al.*, 1996; Tocheva *et al.*, 2006; Board *et al.*, 2008; Dixon and Edwards, 2010b; Meux *et al.*, 2011; Lallement *et al.*, 2014b). Similarly, the majority of tested GSTLs in this study catalyzed the cleavage of GS-pOHPACN to *p*-hydroxyphenyl acetonitrile (Table 1). Uniquely, *Sb*GSTL1 and *Sb*GSTL2 discriminated between GS-pOHPACN 1 and 2, implying that they have evolved to specifically catalyze metabolism of one of the two epimers. Furthermore, their catalytic efficiencies for the preferred substrate were
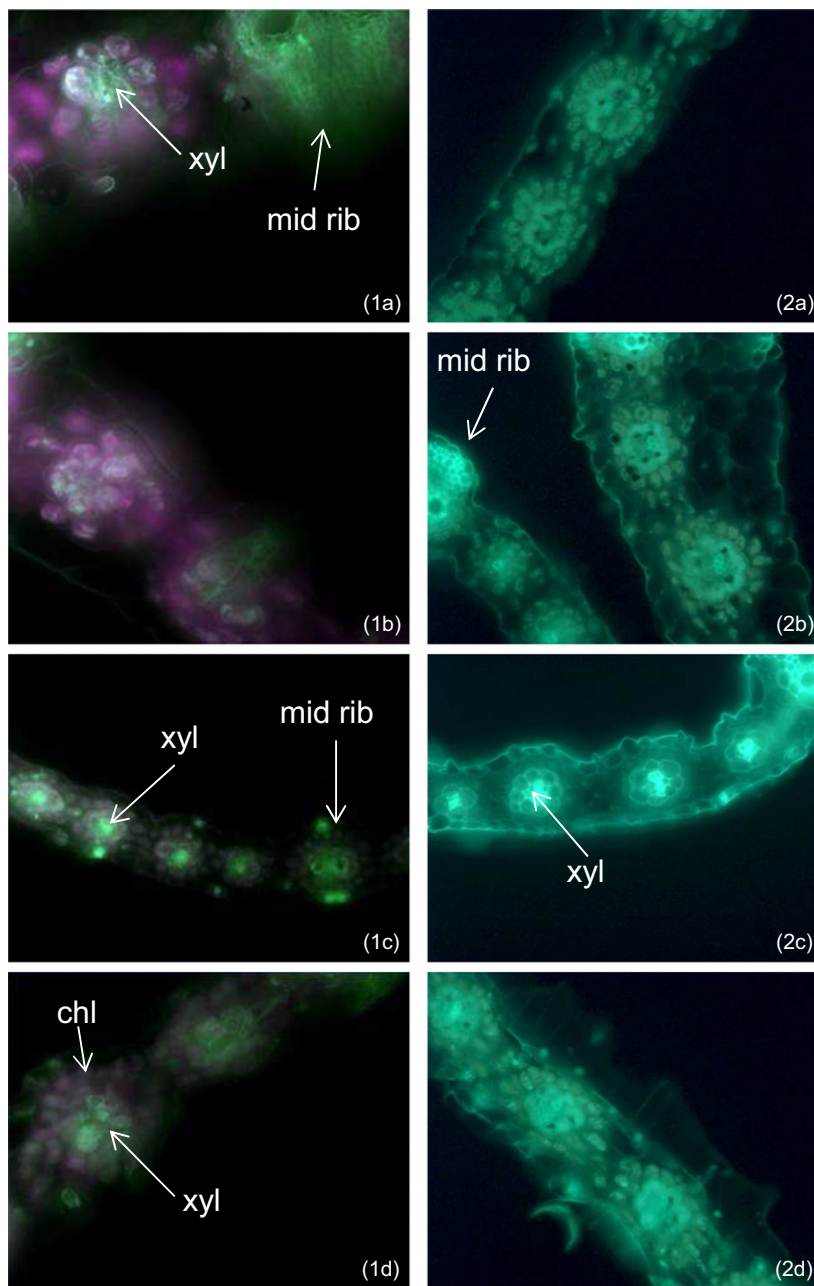
Figure 6. Expression of GSTLs and NIT4s visualized by *in situ* PCR.

Gene expression is visualized as green fluorescence in all images. In some cases, fluorescence pertaining from expression of the genes of interest was challenged by strong chlorophyll and cell wall autofluorescence. Images were therefore captured with two different filters to select the settings that best distinguish between the different sources of fluorescence. In experiment 1 the best images were recorded using the Leica FITC/rhodamine (Fl/RH) filter to differentiate chlorophyll fluorescence (magenta, false color). In experiment 2 the best images were captured with the Leica enhanced GFP filter, providing a stronger green fluorescence from gene expression. chl = chlorophyll, xyl = xylem vessels. Experiment 1: (a) *SbGSTL1*, day 10. (b) *SbGSTL2*, day 10. (c) *SbGSTL4*, day 7. (d) Negative control, day 10. The green xylem cell wall autofluorescence is visualized in the negative control in (1d). This autofluorescence is also strong in images (1a) and (1c). The green structures in the upper right corner of (1a) and lower right corner of (1c) are caused by autofluorescence of the mid rib cell walls. In (1a)–(1c) green fluorescence inside cells that are not xylem vessels corresponds to expression of the respective genes. Experiment 2, all from day 10: (2a) *SbGSTL1*. (2b) *SbNIT4A*. (2c) *SbNIT4B1*. (2d) *SbNIT4B2*. Image (2c) is similar to the negative control of experiment 2 (Figure S6), with only xylem and epidermal cell wall autofluorescence and a weak contribution from chlorophyll visible; in the remaining images green fluorescence not pertaining from epidermal cell walls corresponds mainly to gene expression with only a minor contribution from xylem cell walls. In images from experiment 1, false colors have been applied to avoid red/green comparison. In images from experiment 2, the contrast has been increased to improve visualization. All original images can be viewed in Figure S7.

relatively high compared with the other GSTLs tested. In the study of *in vitro* activity of the three GSTLs found in poplar, the highest catalytic efficiency was found towards the physiologically relevant substrate GS-quercetin (Lallement *et al.*, 2014b). With the most efficient *Pt*GSTL reaching k_{cat}/K_m of 10 μM^{-1} min^{-1} for this substrate, *Sb*GSTL1 and *Sb*GSTL2 are significantly more efficient at converting GS-pOHPACN. The position of *Sb*GSTL1 and *Sb*GSTL2 in the phylogenetic tree of GSTL sequences (Figure 5) supports that these two enzymes have evolved to perform a function not relevant in the other plant species represented in the tree. Dhurrin is present in wheat (Winterberg *et al.*, 2014), but in much reduced amounts compared with sorghum, whereas the remaining plants species do not produce cyanogenic glycosides.

The *in situ* PCR experiments with *Sb*GSTL and *Sb*NIT encoding genes demonstrated similar expression patterns of the mRNAs encoding the enzymes involved in the recycling pathway leading to production of *p*-hydroxyphenylacetic acid (*Sb*GSTL1, *Sb*GSTL2, *Sb*NIT4A, *Sb*NIT4B2) (Figure 6). In contrast, mRNAs encoding the non-related *Sb*GSTL4 and *Sb*NIT4B1 were either localized to different cells than those encoding the genes of the pathway, or they were not detected at the selected time points. In transcriptome analysis of the developing sorghum grain, we found that expression of *Sb*NIT4A and *Sb*NIT4B2 (Nielsen *et al.*, 2016) and accumulation of GS-pOHPACN (Figure S4) increased with dhurrin depletion. Of the 59 GST genes expressed in the developing sorghum grain, expression of *SbGSTL1* showed the highest correlation with the expression profiles of *Sb*NIT4A and *Sb*NIT4B2. The localization of the dhurrin metabolizing enzymes in and around cells of the vascular bundle is consistent with the endogenous recycling pathway providing ammonia and possibly glucose, for distribution within the plant for use in general metabolism. Images of *SbGSTL1* expression were generally easier to obtain than those of *SbGSTL2* expression, indicating that the latter was more weakly expressed, or not always expressed as early as *SbGSTL1*. The sorghum protein activity assays showed that GS-pOHPACN reductive cleaving activity is present from an early stage in seedling development (Figure 4). Presumably, this early activity can be attributed to the clearly expressed *Sb*GSTL1 with expression of the more efficient *Sb*GSTL2 being turned on or increased around the time of maximal dhurrin accumulation where the rate of dhurrin recycling exceeds that of biosynthesis. In the developing sorghum grain, transcripts of both *SbGSTL1* and *SbGSTL2* were relatively highly abundant. However, *SbGSTL2* expression was low in the first phase of grain development and increased dramatically towards grain maturation (Nielsen *et al.*, 2016). Possibly, *Sb*GSTL1 has initially evolved to detoxify and recycle misplaced dhurrin, with the more

efficient isoform eventually evolved to be the main driver of purposeful dhurrin recycling.

Neither *Sb*GSTL3 nor *Ta*GSTL1 were able to catalyze the cleavage of GS-pOHPACN, although they were found to act on other aromatic GS-conjugates (Table 1) (Dixon and Edwards, 2010b). Interestingly, these two enzymes share 77–90% identity with *Os*GSTL1 and *Zm* In2–1 (Figure S4). Together these four enzymes form a distinct cluster in the phylogenetic tree (Figure 5). This situation suggests that they share a function which is conserved across monocots. A striking feature of these four enzymes is that they contain an additional cysteine three residues upstream from the catalytic cysteine (Figure S4). When this additional cysteine residue was mutated in *Ta*GSTL1, the activity towards both aromatic and non-aromatic substrates increased (Dixon and Edwards, 2010b). Its presence is therefore likely to be responsible for the complete lack of activity towards GS-pOHPACN. *Pt*GSTL2 and *Pt*GSTL3 also have an additional cysteine at this position, but are phylogenetically more closely related to other dicot GSTLs, from Arabidopsis.

The epimer specificity of *Sb*GSTL1 and *Sb*GSTL2 towards GS-pOHPACN could suggest that *in planta*, the preceding conversion of dhurrin to GS-pOHPACN is also catalyzed by an enzyme that would usually lead to the formation of only one epimer. The sorghum GSTLs did not catalyze such a reaction, when tested individually or in combination. However, the sorghum grain transcriptome analyses identified four GST transcripts as being highly abundant and strongly correlated with the expression profiles of *Sb*NIT4A/*Sb*NIT4B2 (Nielsen *et al.*, 2016). These will be subject of future studies to test their ability to produce GS-pOHPACN from dhurrin. It is also possible that the conjugation of dhurrin to GS-pOHPACN is a strictly chemical process. Although this reaction produces a 50:50 mixture of (*R*)- and (*S*)-GS-pOHPACN, the epimers were found to isomerize relatively quickly. If the production of GS-pOHPACN is non-enzymatic, the epimer which is not favored as a substrate by the GSTLs might be expected to accumulate in preference to the other epimer. To date, we have been unable to determine the precise stereospecific configuration of the minute amounts of GS-pOHPACN detected in the plant extracts. Alternatively, GS-pOHPACN may be produced by the conjugation of a dhurrin derivative. Previously, three dhurrin-glucosides and two presumed caffeic acid esters of dhurrin have been identified in sorghum (Selmar *et al.*, 1996; Pičmanová *et al.*, 2015), and one of these may serve as substrate for a conjugating GST.

The identified recycling pathway leads to production of *p*-hydroxyphenylacetic acid, which is subsequently glucosylated. This was demonstrated by the production of *p*-glucosyloxyphenylacetic acid from dhurrin administered to leaves of the *tcd1* sorghum mutant (Figure 3a), and from radiolabeled dhurrin formed upon administration of ^{14}C-

labelled tyrosine to wildtype sorghum plants (Figure 3b, c). Not all recycled dhurrin is converted to this glucosylated product (Figure 2). Other presumed products of recycling pathways for cyanogenic glycosides have been identified in sorghum, cassava and almond (Pičmanová *et al.*, 2015; Blomstedt *et al.*, 2016). The ^{14}C-experiment revealed only minor production of other labelled compounds than dhurrin and *p*-glucosyloxyphenylacetic acid (Figure S2), none of which could be identified. However, this experiment was terminated at 11 days, and it is therefore possible that these other presumed products of dhurrin metabolism are produced later. The total amount of ^{14}C in the plant extracts decreased by 40% over the course of 8 days (Figure 3c). This result demonstrated that not only the nitrogen, but also the carbon originally invested in dhurrin is recycled, e.g. into non-methanol extractable polymers such as protein and lignin, or into root biomass. This situation in turn indicated that the remaining fraction of *p*-glucosyloxyphenylacetic acid serves a specific purpose. *p*-Hydroxyphenylacetic acid has been shown to have growth promoting and other auxin-like effects in plants and algae (Abe *et al.*, 1974; Fries and Iwasaki, 1976; Ding *et al.*, 2008; Simon and Petrášek, 2011), and auxin homeostasis is controlled by glucosylation (Korasick *et al.*, 2013). Consequently, it is plausible that *p*-glucosyloxyphenylacetic acid is an inactive storage form of a signaling compound in sorghum.

Several cyanogenic plant species are polymorphic for the production of cyanogenic glucosides or exist as naturally mutated sub-species that do not accumulate them (Crawford-Sidebotham, 1972; Gleadow *et al.*, 2003; Sanchez-Perez *et al.*, 2008; Lai *et al.*, 2014). These defense compounds have therefore traditionally not been considered as compounds contributing to other aspects of plant fitness and physiology, but this assumption has been questioned (Swain and Poulton, 1994; Neilson *et al.*, 2013; Gleadow and Møller, 2014). The use of chemically induced mutations or biotechnological approaches to knock out or reduce cyanogenic glucoside biosynthesis in sorghum and cassava has demonstrated that under specific developmental conditions these plants may show impaired growth (Jørgensen *et al.*, 2005; Blomstedt *et al.*, 2012). The identification of a dhurrin recycling system for recovery of compounds useful for general metabolism, as well as production of a metabolite with putative roles in signaling corroborates the proposed multi-functionality of cyanogenic glucosides and exemplifies how general and specialized metabolism in plants should be envisioned as one highly dynamic and integrated metabolic system. The catalytic repertoire of the GST superfamily of enzymes is extremely versatile (Dixon and Edwards, 2010a; Dixon *et al.*, 2010; Labrou *et al.*, 2015) and the number of identified plant GST functions that do not include detoxification and redox homeostasis is increasing. The identification of GST involvement in cyanogenic glucoside recycling underpins that members of this enzyme family should be considered as potential key players in the intimate interplay between general and specialized metabolism.

EXPERIMENTAL PROCEDURES

Plant material and sampling

The *S. bicolor* cultivar SS1000 was used for all experiments, except administration of unlabeled dhurrin (see below). Seeds were soaked in water for 24 h and sown on top of wet gauze-covered soil (to ensure uniform length of the mesocotyls). The pots were covered with perforated cling film and germinated in a climate chamber (28°C/25°C day/night, 16 h light, 80% humidity, light intensity 480 μmol m^{-2} sec^{-2}). After 3 days cling film and non-germinated seeds were removed. Furthermore, preliminary results showed that at the early stages, dhurrin content was positively correlated with plant size. Therefore the population was trimmed by removing both the most developed and least developed plants and plants that differed visually from the majority (curled leaves, torn leaves etc.). Each sample replicate consisted of all above-ground material from a single plant, i.e. hypocotyl, node, coleoptile and all leaves, leaf sheaths and possible crown shoots. For administration of dhurrin, seed of the EMS mutant total cyanide deficient (*tcd1*) line and, as control, the parent line (Blomstedt *et al.*, 2012) were soaked in water for 24 h, sown on wet soil and covered by a thin layer of moist soil and grown in a greenhouse (28°/25°C d/n). In both experiments, the harvested plants were visually selected to be at an average growth stage of all plants in the pot, i.e. an average number of fully unfolded leaves and average height. All samples were immediately frozen in liquid nitrogen at harvest.

Metabolism of dhurrin and L-[U-^{14}C]-tyrosine in sorghum leaves

Dhurrin was administered to leaves of the sorghum *tcd1* mutant line and the parent line. The third and second leaves of 7-day-old and 14-day-old plants were excised a few mm below the leaf blade and immediately placed in tubes containing either 500 nmol dhurrin in 50 μl water or 50 μl water, with the few mm of leaf sheath carefully immersed in the solution, and placed under ventilation in a fume hood to promote uptake. As t = 0 controls, leaves of each plant line/age/leaf number were frozen in liquid nitrogen at harvest. All experiments were carried out in triplicate. After uptake, the leaves were transferred to larger tubes containing 500 μl water. The lids were closed, and the leaves allowed to metabolize for 5 h, before they were removed from the water, frozen in liquid nitrogen and subsequently extracted and analyzed by LC-MS as described below. For administration of L-[U-^{14}C]-tyrosine, SS1000 seedlings were removed from the soil 5 days after sowing (2½ leaf stage) and the roots cut approximately 2 cm below the seed to facilitate reproducible uptake across replicates. Each plant was placed in a tube with the cut roots immersed in 50 μl water containing 2.5 μCi of L-[U-^{14}C]-tyrosine (391 mCi/mmol, Larodan Fine Chemicals). Control plant roots were immersed in water containing an identical concentration of unlabeled L-tyrosine. After uptake, 50 μl water was added to the tubes for rinsing, and when this was also taken up the plants were transplanted back into wet soil to resume growth. The plants were initially affected by the procedure, but after a few days resumed growth and grew normally for the remainder of the period, only 1–2 days delayed compared to undisturbed plants. The plants were harvested in triplicate on day 3, 6 and 11 after uptake and separated into leaf 2 and the remaining tissue, and each part

extracted separately, as described below. For determination of total ^{14}C and labeled dhurrin, aliquots of each plant part were combined. Total-^{14}C was measured on a Trilux 1450 MicroBeta liquid scintillation counter (Wallac). Total dhurrin was visualized by TLC analysis using Silica Gel 60 F$_{254}$ plates from *Merck* and ethylacetate:acetone:water:formic acid (20:70:20:0.5) as elution solvent. All individual extracts were also analyzed by this TLC-system and in one allowing separation of *p*-hydroxyphenyl acetonitrile, *p*-hydroxyphenylacetic acid and *p*-hydroxybenzaldehyde using a mobile phase of toluene:ethylacetate:methanol:formic acid (83:17:2:0.5). After sample loading and drying, all plates were initially eluted 2 cm in 100% MeOH to focus the origin, and dried again before elution in separation solvent. Radiolabeled products were visualized by exposure of phosphor imager screens from Molecular Dynamics, which were developed using a STORM 840 phosphor imager (Amersham Biosciences). Spots were quantified using the Imagequant software (Amersham Biosciences).

Extraction of metabolites

The frozen plant samples were extracted for 2×3 min in boiling 85% MeOH containing 0.5% formic acid to stabilize dhurrin and prevent the GSH–dhurrin chemical reaction. The extraction solvent was added straight to the frozen samples which were immediately transferred to a boiling water bath; nodes and leaf sheaths from large plants were first coarsely ground in liquid nitrogen to ensure complete extraction and immediate quenching of metabolism. The extracts were decanted off and kept at $-20°$C until analysis.

Chemical standards and substrates

p-Hydroxyphenylacetonitrile, *p*-hydroxyphenylacetic acid, *p*-hydroxyphenylacetamide and *p*-hydroxybenzaldehyde were purchased from Sigma, and dhurrin (Møller *et al.*, 2016) and 4-NPG (Board *et al.*, 2008) synthesized as described. GS-pOHPACN was synthesized by mixing approximately 80 mmol dhurrin 1:1 with reduced GSH (Sigma) in 200 mM KP$_i$ (adjusted to pH 8 with NaOH) and shaken for 3 h at 37°C. The resulting mixture was pre-fractioned on Strata-X 33 μm Polymeric reversed phase SPE columns (Phenomenex): 3 ml columns containing 500 mg column material were conditioned with 10 ml methanol and equilibrated with 10 ml MilliQ-water, 7.5 ml crude GS-pOHPACN mix was applied to each column, followed by 10 ml MilliQ-water for washing, and the GS-pOHPACN was eluted in 5 ml methanol. This eluate was fractionated on a preparative HPLC from Shimadzu consisting of LC-20AT quarternary pump, CBM-20 communication module, SIL-10AP autosampler, SPD-M20A diode array detector, FRC-10 A fraction collector and two sample coolers to keep samples and fractions cold. The column was a Zorbax SB-C18, 9.4 mm i.d, 150 mm, 5 μm particles (Agilent). The two mobile phases were: A = 0.1% formic acid, and B = 80% acetonitrile, 0.1% formic acid, the flow rate was 7 ml/min, and the gradient program was as follows: 0–10 min: B = 10%, 10–12.5 min: B = linear gradient 10–100%, 12.5–15 min: B = linear gradient 100–10%, followed by 10 min equilibration. The yield was on the order of a few percent, but the procedure was not optimized and could most likely benefit from a better pH control during incubation. The GS-pOHPACN structures were verified by LC-MS (Figure S3) and NMR. The ^{1}H and ^{13}C NMR spectra were recorded on a Bruker Advance 400 spectrometer at 400 and 101 MHz, respectively. NMR peak assignments were established by NOESY, COSY, HSQC and HMBC methods. For full assignments of the chemical shifts of the two GS-pOHPACN epimers, see Table S1. In brief, the chemical shifts for the GSH part of the molecules were consistent with those previously reported

(Geu-Flores *et al.*, 2009). Furthermore, the ^{1}H NMR data of the dhurrin-derived part of the molecules revealed that the aromatic protons appeared as a characteristic AB-system of multiplets at δ 7.41 & δ 6.94 ppm (d, $J = 8.6$ Hz) for epimer 1 and at δ 7.40 & δ 6.94 ppm (d, $J = 8.6$ Hz) for epimer 2. This demonstrates the maintenance of the aromatic substitution pattern of the aglycones of (*S*)-dhurrin and its epimer (*R*)-taxiphyllin (Seigler *et al.*, 2005; Møller *et al.*, 2016). Conversely, the epimeric proton at the CN-bearing carbon (Figure S3) for both epimers was more shielded and appeared as a singlet resonating upfield (δ 5.25 and δ 5.24) compared with dhurrin and taxiphyllin (δ 5.91 and δ 5.79), demonstrating that this carbon is linked to the S-atom of the glutathione molecule. That the CN group is retained in the structure was documented by its diagnostic chemical shift at δ 120.1 ppm for both epimers.

Extraction of soluble protein from sorghum

For each time point, several plants were pooled, ground in liquid nitrogen and 10% (m/m) polyvinyl poly pyrrolidone (PVPP from Sigma) was added, followed by approximately 3 volumes (m/v) ice cold 50 mM KP$_i$ (adjusted to pH 7.5 with NaOH) containing 3 mM ethylenediamine-tetra-acetic acid (EDTA), 1 mM phenylmethylsulfonyl fluoride (PMSF) and 1 mM GSH to keep nitrilases reduced. The slurries were filtered through muslin gauze and the insoluble fractions removed by centrifugation, first 20 min at 5000 *g*, followed by 30 min at 100 000 *g* of the supernatants from the first centrifugation. The final supernatants were desalted with PD10 columns (GE Healthcare, Brøndby, Denmark), following the protocol using 5 mM KP$_i$ (adjusted to pH 7.5 with NaOH) with 1 mM GSH as desalting buffer. The extracts were either used immediately or frozen in liquid nitrogen and stored at $-80°$C until assayed.

Sequence verification and analyses

The previously identified sequences for three putative *Sb*DHAR enzymes and four putative *Sb*GSTLs (see accession numbers below) were tentatively confirmed by search in EST databases, and the expressed GSTL sequences were verified by cloning from cDNA (3-day-old seedlings, iScript cDNA synthesis kit from Bio-Rad, primer pair sequences in Table S3). The online software tool TargetP 1.1 (http://www.cbs.dtu.dk/services/TargetP/) (Nielsen *et al.*, 1997; Emanuelsson *et al.*, 2000) identified a chloroplast targeting signal (first 15 aa) in the translated protein sequence of MF770506 (*Sb*GSTL4) with high probability (cTP = 0.961, RC = 1). Phylogenetic analysis was performed with the software MEGA 6.06 (Tamura *et al.*, 2013): GSTL protein sequences were aligned using MUSCLE (Edgar, 2004) at default settings (Data S1), and the alignment was used to calculate overall sequence percent identities between proteins using the software CLC Main Workbench 7.02 (Figure S5). The same full-length sequences were aligned with *At*DHAR1 as outgroup for construction of a maximum likelihood phylogenetic tree by MEGA 6.06 (Data S2). The Analyses Preferences function was first used to decide which model is considered to describe the observed substitution pattern best [the model with the lowest BIC score (Bayesian information criterion)], and the tree was then constructed using 1000 bootstraps, JTT model and a discrete gamma distribution.

Expression and purification of enzymes

Synthetic genes, codon optimized for expression in *E. coli*, of the three *SbGSTDHAR* sequences, four *SbGSTL* sequences and a truncated version of *SbGSTL4*, *SbΔGSTL4* with the first 15 aa removed, were purchased from GenScript. These were subcloned into the *E. coli* pET-STRP3 expression vector to add a Strep3 tag

to the proteins (Brazier-Hicks *et al.*, 2007), expressed in BL21(DE3) cells (Novagen, Merch Group, Hellerup, Denmark) and purified as described (Dixon *et al.*, 2009) with the only modifications that the cells were grown in TB broth, and the pellets resuspended in 50 mm KP_i (adjusted to 7.5 with NaOH).

Enzyme assays and determination of Michaelis–Menten parameters

The protein content of soluble plant protein samples was estimated from the absorbance at 280 nm measured with a NanoDrop ND-1000 spectrophotometer (NanoDrop Technologies, ThermoFisher Scientific, Roskilde, Denmark) and the concentrations adjusted to 1 mg/l in desalting buffer. Of this, 80 μl was mixed with 10 μl substrate solutions (25 mm dhurrin or 2 mm GS-pOHPACN 1 or 2) and 10 μl 30 mm GSH in 40 mm KP_i (adjusted to 7.5 with NaOH) to make the final concentrations respectively 2.5 or 0.2 mm (substrate), 3 mm (GSH) and 8 mm (KP_i). The samples were incubated at 37°C for 5 or 45 min and the assays stopped by adding 1 volume MeOH containing 1% formic acid. The samples were analyzed by LC-MS. GSTL enzyme activity assays were carried out in a modified version of the coupled assay previously described (Edwards and Dixon, 2005), using a Shimadzu UV-2550 UV-VIS spectrophotometer. The activities of the enzymes were measured by the consumption of NADPH (340 nm, $\varepsilon = 6200$ M^{-1} cm^{-1}) by glutathione reductase as it reduces the oxidized GSH produced when the GSTLs cleave GSH conjugates, using the following solutions: A, 200 mm KP_i + 4 mm EDTA (adjusted to pH 7.5 with NaOH); B, 2.5 mm NADPH in 0.1% $NAHCO_3$; C, 20 mm GSH (adjusted to pH 6 with NaOH); and D, 6 U/ml GSH reductase (EC 1.6.4.2 from Sigma) in solution A. In a plastic cuvette 600 μl A (30°C) and 100 μl each of B, C and D were mixed and allowed to incubate at 30°C to reduce any oxidized GSH present. After 2 min, 50 μl enzyme solution was added and incubated for an extra 20 sec, after which 50 μl substrate solution was added, and the change in absorbance was measured for 2 min. In the assays, the amount of enzyme was between 0.2–15 μg and substrate concentrations were between 1–250 μm. For the reference compound 4NPG the general procedure was the same, but the reaction rate was measured as the change in 4NPG-concentration at 305 nm ($\varepsilon = -1100$ M^{-1} cm^{-1}) (Board *et al.*, 2008), the mixture was 800 μl A, 100 μl B, 50 μl enzyme, 50 μl substrate, and the substrate concentrations were 20–500 μm. The absorbance at 280 nm of dilution series of enzyme was measured using a NanoDrop spectrophotometer, and extinction coefficients of the Strep3 tagged proteins were estimated using the ProtParam tool found at http://web.expasy.org. The apparent k_{cat} and K_m values were calculated with the SigmaPlot 12.5 software using a non-linear single substrate Michaelis–Menten regression model. The activity assays of *Sb*GSTL1–*Sb*GSTL4 towards GS-pOHPACN and 4-NPG were performed in respectively three and two series of technical replicates.

LC-MS analyses of plant extracts and enzyme assay samples

Plant and enzyme assay samples were analyzed by two different LC-MS procedures. All samples were diluted appropriately in MilliQ-water to make the concentrations fall within the standard curves and filtered through 0.45-μm Multiscreen HTS HV filters (Millipore). For detection of dhurrin, *p*-glucosyloxyphenylacetic acid and GS-pOHPACN in plant extracts and for analysis of the purified GS-pOHPACN epimers, samples were analyzed as previously described (Pičmanová *et al.*, 2015) using an Agilent 1100 Series LC (Agilent Technologies, Waldbronn, Germany) coupled to a Bruker HCT-Ultra ion trap mass spectrometer (Bruker Daltonics, Bremen, Germany) in positive mode ESI (ElectroSpray Ionization). The compounds were quantified using standard curves in the range 0.1–400 μm. To study dhurrin metabolism in solutions of plant protein extracts (Figure 4), dhurrin, GS-pOHPACN, *p*-hydroxyphenyl acetonitrile, *p*-hydroxyphenylacetic acid, *p*-hydroxyphenylacetamide and *p*-hydroxybenzaldehyde were analyzed in a targeted approach using UPLC-triple quad-MS/MS in either negative or positive mode ESI (details in Experimental Methods S1), with standard curves in the range 0.02–25 μm.

In situ PCR

The third leaf blades from 7-day-old and 10-day-old plants were used for *in situ* analysis of gene expression localization following the procedure previously described (Jørgensen *et al.*, 2005, 2011) which is modified from that of Koltai and Bird (2000). Primers were added according to the gene to be tested (primer sequences in Table S3) and the primer specificities were validated by DNA sequencing of the respective PCR products. The parameters for the PCR reaction were: 2 min at 90°C, then 35 cycles at 92°C for 30 sec, 60°C for 30 sec and 72°C for 60 sec, and finally 30–60 min at 12°C. In the PCR reaction dUTP labelled with digoxigenin (DIG) (Roche, Hvidovre, Denmark) was incorporated into the PCR products, and the gene expression was visualized with a DIG-specific antibody conjugated with fluorescein isothiocyanate (FITC) (Roche). The sections were finally embedded in anti-fading agent (Citiflour) and examined by a Leica DMR HC fluorescence microscope and photographed with a Leica DC 300F camera. The images presented from experiment 1 were recorded using the FITC/rhodamine (FI/RH) excitation/emission filters, respectively BP 490/15 and BP605/30, to differentiate chlorophyll autofluorescence from gene expression. In experiment 2 the enhanced GFP filter with excitation filter BP 470/40 and emission filter BP 525/50 was used.

ACCESSION NUMBERS

GSTL sequence data from this article can be found in the GenBank data libraries under accession numbers (Phytozome identifiers in brackets): *Sb*GSTL1: MF770503 (Sobic.002G421200.2), *Sb*GSTL2: MF770504 (Sobic.009G033200.2), *Sb*GSTL3: MF770505 (Sobic.001G412700.1) *Sb*GSTL4: MF770506 (Sobic.001G412800.2). The sequences of the expressed *Sb*DHAR coding sequences were not experimentally verified. The sequences used correspond to those provided by Lallement *et al.* (2014a) with Phytozome identifier numbers from version 10 of this database: Sb10 g008310, Sb09 g001700, Sb09 g001690.

AUTHOR CONTRIBUTIONS

N.B. and B.L.M. designed the experiments and wrote the paper, N.B. performed the majority of experiments and analyses; in addition E.H.N., C.C., and C.E.O. performed

some of the LC-MS analyses and data handling, M.S.M. and C.E.O. carried out and interpreted NMR experiments, and K.J. carried out and analyzed *in situ* PCR. D.P.D., R.E., C.C., M.S.M. and C.E.O. provided analytical tools and/or specific scientific advice, and all authors have read and commented on the manuscript.

CONFLICT OF INTEREST

The authors declare no conflict of interest.

SUPPORTING INFORMATION

Additional Supporting Information may be found in the online version of this article.

Figure S1. Production of *p*-glucosyloxyphenylacetic acid in excised sorghum leaves upon administration of dhurrin.

Figure S2. Metabolism of L-[U-^{14}C]-tyrosine in sorghum plants.

Figure S3. Structure elucidation of GS-pOHPACN.

Figure S4. GS-pOHPACN in the developing sorghum grain.

Figure S5. Subset of sequence alignment and percent identities of GSTL sequences from different plants.

Figure S6. Expression of *GSTL*s visualized by *in situ* PCR.

Figure S7. Expression of GSTLs and NIT4s; original images from Figure 6.

Table S1. Complete ^{1}H NMR and ^{13}C chemical shift assignments for purified GS-pOHPACN.

Table S2. Turnover numbers of Arabidopsis and wheat GSTLs' activities towards GS-pOHPACN.

Table S3. Primers for cloning *GSTL*s from sorghum cDNA and for *in situ* PCR analysis of *GSTL* and *NIT4* expression.

Methods S1. UHPLC-triple quadrupole-MS/MS analyses of assays with plant protein.

Data S1. Full sequence alignment of GSTLs from different plants.

Data S2. Full sequence alignment of GSTLs from different plants, including *At*DHAR1 as outgroup

REFERENCES

Abe, H., Uchiyama, M. and Sato, R. (1974) Isolation of phenylacetic acid and its para-hydroxy derivative as auxin-like substances from *Undaria Finnatifida. Agr Biol Chem*, **38**, 897–898.

Adewusi, S.R.A. (1990) Turnover of dhurrin in green sorghum seedlings. *Plant Physiol*. **94**, 1219–1224.

Agerbirk, N., Warwick, S.I., Hansen, P.R. and Olsen, C.E. (2008) *Sinapis* phylogeny and evolution of glucosinolates and specific nitrile degrading enzymes. *Phytochemistry*, **69**, 2937–2949.

Blomstedt, C.K., Gleadow, R.M., O'Donnell, N. *et al.* (2012) A combined biochemical screen and TILLING approach identifies mutations in *Sorghum bicolor* L. Moench resulting in acyanogenic forage production. *Plant Biotechnol. J.* **10**, 54–66.

Blomstedt, C.K., O'Donnell, N.H., Bjarnholt, N., Neale, A.D., Hamill, J.D., Møller, B.L. and Gleadow, R.M. (2016) Metabolic consequences of knocking out UGT85B1, the gene encoding the glucosyltransferase required for synthesis of dhurrin in *Sorghum bicolor* (L. Moench). *Plant Cell Physiol*. **57**, 373–386.

Board, P.G., Coggan, M., Cappello, J., Zhou, H., Oakley, A.J. and Anders, M.W. (2008) *S*-(4-Nitrophenacyl)glutathione is a specific substrate for glutathione transferase omega 1–1. *Anal. Biochem.* **374**, 25–30.

Brazier-Hicks, M., Offen, W.A., Gershater, M.C., Revett, T.J., Lim, E.-K., Bowles, D.J., Davies, G.J. and Edwards, R. (2007) Characterization and engineering of the bifunctional *N*- and *O*-glucosyltransferase involved in xenobiotic metabolism in plants. *PNAS*, **104**, 20238–20243.

Busk, P.K. and Møller, B.L. (2002) Dhurrin synthesis in sorghum is regulated at the transcriptional level and induced by nitrogen fertilization in older plants. *Plant Physiol*. **129**, 1222–1231.

Chen, K., Dugas, T.R. and Cole, R.B. (2008) Liquid chromatography-electrospray tandem mass spectrometry investigations of fragmentation pathways of biliary 4,4′-methylenedianiline conjugates produced in rats. *Anal. Bioanal. Chem.* **391**, 271.

Chi, Y.H., Cheng, Y., Vanitha, J., Kumar, N., Ramamoorthy, R., Ramachandran, S. and Jiang, S.Y. (2011) Expansion mechanisms and functional divergence of the glutathione S-transferase family in sorghum and other higher plants. *DNA Res*. **18**, 1–16.

Crawford-Sidebotham, T.J. (1972) Role of slugs and snails in maintenance of cyanogenesis polymorphisms of *Lotus corniculatus* and *Trifolium repens. Heredity*, **28**, 405–411.

Crush, J.R. and Caradus, J.R. (1995) Cyanogenesis potential and iodine concentration in white clover (*Trifolium repens* L) cultivars. *New Zeal J Agr Res*, **38**, 309–316.

Cummins, I., Dixon, D.P., Freitag-Pohl, S., Skipsey, M. and Edwards, R. (2011) Multiple roles for plant glutathione transferases in xenobiotic detoxification. *Drug Met Rev*, **43**, 266–280.

Ding, L., Qin, S., Li, F., Chi, X. and Laatsch, H. (2008) Isolation, antimicrobial activity, and metabolites of fungus *Cladosporium* sp. associated with red alga *Porphyra yezoensis. Curr. Microbiol*. **56**, 229–235.

Dixon, D.P. and Edwards, R. (2010a) Glutathione transferases. *Arabidopsis Book*, **8**, e0131.

Dixon, D.P. and Edwards, R. (2010b) Roles for stress-inducible Lambda glutathione transferases in flavonoid metabolism in plants as identified by ligand fishing. *J. Biol. Chem*. **285**, 36322–36329.

Dixon, D.P., Davis, B.G. and Edwards, R. (2002) Functional divergence in the glutathione transferase superfamily in plants - Identification of two classes with putative functions in redox homeostasis in *Arabidopsis thaliana. J. Biol. Chem.* **277**, 30859–30869.

Dixon, D.P., Hawkins, T., Hussey, P.J. and Edwards, R. (2009) Enzyme activities and subcellular localization of members of the *Arabidopsis* glutathione transferase superfamily. *J. Exp. Bot.* **60**, 1207–1218.

Dixon, D.P., Skipsey, M. and Edwards, R. (2010) Roles for glutathione transferases in plant secondary metabolism. *Phytochemistry*, **71**, 338–350.

Edgar, R.C. (2004) MUSCLE: multiple sequence alignment with high accuracy and high throughput. *Nucleic Acids Res.* **32**, 1792–1797.

Edwards, R. and Dixon, D.P. (2005) *Plant glutathione transferases*. San Diego: Elsevier Academic Press Inc.

Emanuelsson, O., Nielsen, H., Brunak, S. and von Heijne, G. (2000) Predicting subcellular localization of proteins based on their *N*-terminal amino acid sequence. *J. Mol. Biol.* **300**, 1005–1016.

Fedrizzi, B., Guella, G., Perenzoni, D., Gasperotti, M., Masuero, D., Vrhovsek, U. and Mattivi, F. (2012) Identification of intermediates involved in the biosynthetic pathway of 3-mercaptohexan-1-ol conjugates in yellow passion fruit (*Passiflora edulis f. flavicarpa*). *Phytochemistry*, **77**, 287–293.

Forslund, K., Morant, M., Jørgensen, B., Olsen, C.E., Asamizu, E., Sato, S., Tabata, S. and Bak, S. (2004) Biosynthesis of the nitrile glucosides rhodiocyanoside A and D and the cyanogenic glucosides lotaustralin and linamarin in *Lotus japonicus. Plant Physiol.* **135**, 71–84.

Fries, L. and Iwasaki, H. (1976) *p*-Hydroxyphenylacetic acid and other phenolic compounds as growth stimulators of red alga *Porphyra tenera. Plant Sci Lett*, **6**, 299–307.

Geu-Flores, F., Nielsen, M.T., Nafisi, M., Moldrup, M.E., Olsen, C.E., Motawia, M.S. and Halkier, B.A. (2009) Glucosinolate engineering identifies gamma-glutamyl peptidase. *Nature Chem Biol*, **5**, 575–577.

Geu-Flores, F., Moldrup, M.E., Bottcher, C., Olsen, C.E., Scheel, D. and Halkier, B.A. (2011) Cytosolic gamma-glutamyl peptidases process glutathione conjugates in the biosynthesis of glucosinolates and camalexin in *Arabidopsis. Plant Cell*, **23**, 2456–2469.

Gleadow, R.M. and Møller, B.L. (2014) Cyanogenic glycosides: synthesis, physiology, and phenotypic plasticity. *Annu. Rev. Plant Biol.* **65**, j155–j185.

Gleadow, R.M. and Woodrow, I.E. (2000) Temporal and spatial variation in cyanogenic glycosides in *Eucalyptus cladocalyx. Tree Physiol*. **20**, 591–598.

Gleadow, R.M., Veechies, A.C. and Woodrow, I.E. (2003) Cyanogenic *Eucalyptus nobilis* is polymorphic for both prunasin and specific beta-glucosidases. *Phytochemistry*, **63**, 699–704.

Hartmann, T.N., Fricker, M.D., Rennenberg, H. and Meyer, A.J. (2003) Cell-specific measurement of cytosolic glutathione in poplar leaves. *Plant Cell Env*, **26**, 965–975.

Hershey, H.P. and Stoner, T.D. (1991) Isolation and characterization of cDNA clones for RNA species induced by substituted benzenesulfonamides in corn. *Plant Mol. Biol.* **17**, 679–690.

Huang, Y., Xun, R.D., Chen, G.J. and Xun, L.Y. (2008) Maintenance role of a glutathionyl-hydroquinone lyase (PcpF) in pentachlorophenol degradation by *Sphingobium chlorophenolicum* ATCC 39723. *J. Bacteriol.* **190**, 7595–7600.

Jain, M., Ghanashyam, C. and Bhattacharjee, A. (2010) Comprehensive expression analysis suggests overlapping and specific roles of rice glutathione S-transferase genes during development and stress responses. *BMC Genom.* **11**, 73. https://doi.org/10.1186/1471-2164-11-73.

Jenrich, R., Trompetter, I., Bak, S., Olsen, C.E., Møller, B.L. and Piotrowski, M. (2007) Evolution of heteromeric nitrilase complexes in Poaceae with new functions in nitrile metabolism. *PNAS*, **104**, 18848–18853.

Jørgensen, K., Bak, S., Busk, P.K., Sørensen, C., Olsen, C.E., Puonti-Kaerlas, J. and Møller, B.L. (2005) Cassava plants with a depleted cyanogenic glucoside content in leaves and tubers. Distribution of cyanogenic glucosides, their site of synthesis and transport, and blockage of the biosynthesis by RNA interference technology. *Plant Physiol.* **139**, 363–374.

Jørgensen, K., Morant, A.V., Morant, M., Jensen, N.B., Olsen, C.E., Kannangara, R., Motawia, M.S. and Møller, B.L. (2011) Biosynthesis of the cyanogenic glucosides linamarin and lotaustralin in cassava: isolation, biochemical characterization, and expression pattern of CYP71E7, the oxime-metabolizing cytochrome P450 enzyme. *Plant Physiol.* **155**, 282–292.

Kobayashi, H., Takase, H., Suzuki, Y., Tanzawa, F., Takata, R., Fujita, K., Kohno, M., Mochizuki, M., Suzuki, S. and Konno, T. (2011) Environmental stress enhances biosynthesis of flavor precursors, S-3-(hexan-1-ol)-glutathione and S-3-(hexan-1-ol)-L-cysteine, in grapevine through glutathione S-transferase activation. *J. Exp. Bot.* **62**, 1325–1336.

Koltai, H. and Bird, D.M. (2000) High throughput cellular localization of specific plant mRNAs by liquid-phase *in situ* reverse transcription-polymerase chain reaction of tissue sections. *Plant Physiol.* **123**, 1203–1212.

Korasick, D.A., Enders, T.A. and Strader, L.C. (2013) Auxin biosynthesis and storage forms. *J. Exp. Bot.* **64**, 2541–2555.

Kumar, S., Asif, M.H., Chakrabarty, D., Tripathi, R.D., Dubey, R.S. and Trivedi, P.K. (2013) Differential expression of rice Lambda class GST gene family members during plant growth, development, and in response to stress conditions. *Plant Mol. Biol. Rep.* **31**, 569–580.

Labrou, N.E., Papageorgiou, A.C., Pavli, O. and Flemetakis, E. (2015) Plant GSTome: structure and functional role in xenome network and plant stress response. *Curr. Opin. Biotechnol.* **32**, 186–194.

Lai, D., Abou Hachem, M., Robson, F., Olsen, C.E., Wang, T.L., Møller, B.L., Takos, A.M. and Rook, F. (2014) The evolutionary appearance of non-cyanogenic hydroxynitrile glucosides in the *Lotus* genus is accompanied by the substrate specialization of paralogous beta-glucosidases resulting from a crucial amino acid substitution. *Plant J.* **79**, 299–311.

Lallement, P.-A., Brouwer, B., Keech, O., Hecker, A. and Rouhier, N. (2014a) The still mysterious roles of cysteine-containing glutathione transferases in plants. *Front Pharmacol*, **5**, 192. https://doi.org/10.3389/fphar.2014.00192.

Lallement, P.A., Meux, E., Gualberto, J.M., Prosper, P., Didierjean, C., Saul, F., Haouz, A., Rouhier, N. and Hecker, A. (2014b) Structural and enzymatic insights into Lambda glutathione transferases from *Populus trichocarpa*, monomeric enzymes constituting an early divergent class specific to terrestrial plants. *Biochem J.* **462**, 39–52.

Lan, T., Yang, Z.-L., Yang, X., Liu, Y.-J., Wang, X.-R. and Zeng, Q.-Y. (2009) Extensive functional diversification of the populus glutathione S-transferase supergene family. *Plant Cell*, **21**, 3749–3766.

Lieberei, R., Selmar, D. and Biehl, B. (1985) Metabolization of cyanogenic glucosides in *Hevea brasiliensis*. *Plant Syst. Evol.* **150**, 49–63.

Liu, Y.J., Han, X.M., Ren, L.L., Yang, H.L. and Zeng, Q.Y. (2013) Functional divergence of the glutathione S-transferase supergene family in *Physcomitrella patens* reveals complex patterns of large gene family evolution in land plants. *Plant Physiol.* **161**, 773–786.

Mao, C.H. and Anderson, L. (1965) Cyanogenesis in *Sorghum vulgare*. 2. Mechanism of alkaline hydrolysis of dhurrin (*p*-hydroxymandelonitrile glucoside). *J. Org. Chem.* **30**, 603–607.

McCarthy, D.L., Navarrete, S., Willett, W.S., Babbitt, P.C. and Copley, S.D. (1996) Exploration of the relationship between tetrachlorohydroquinone dehalogenase and the glutathione S-transferase superfamily. *Biochemistry*, **35**, 14634–14642.

Meux, E., Prosper, P., Ngadin, A., Didierjean, C., Morel, M., Dumarcay, S., Lamant, T., Jacquot, J.P., Favier, F. and Gelhaye, E. (2011) Glutathione transferases of *Phanerochaete chrysosporium* S-glutathionyl-*p*-hydroquinone reductase belongs to a new structural class. *J. Biol. Chem.* **286**, 9162–9173.

Meyer, A.J., May, M.J. and Fricker, M. (2001) Quantitative *in vivo* measurement of glutathione in *Arabidopsis* cells. *Plant J.* **27**, 67–78.

Miller, J.M. and Conn, E.E. (1980) Metabolism of hydrogen cyanide by higher plants. *Plant Physiol.* **65**, 1199–1202.

Møller, B.L. (2010) Functional diversifications of cyanogenic glucosides. *Curr. Opin. Plant Biol.* **13**, 338–347.

Møller, B.L., Olsen, C.E. and Motawia, M.S. (2016) General and stereocontrolled approach to the chemical synthesis of naturally occurring cyanogenic glucosides. *J. Nat. Prod.* **79**, 1198–1202.

Neilson, E.H., Goodger, J.Q.D., Motawia, M.S., Bjarnholt, N., Frisch, T., Olsen, C.E., Møller, B.L. and Woodrow, I.E. (2011) Phenylalanine derived cyanogenic diglucosides from *Eucalyptus camphora* and their abundances in relation to ontogeny and tissue type. *Phytochemistry*, **72**, 2325–2334.

Neilson, E.H., Goodger, J.Q.D., Woodrow, I.E. and Møller, B.L. (2013) Plant chemical defense: at what cost? *Trends Plant Sci.* **18**, 250–258.

Nielsen, H., Engelbrecht, J., Brunak, S. and von Heijne, G. (1997) Identification of prokaryotic and eukaryotic signal peptides and prediction of their cleavage sites. *Prot eng.* **10**, 1–6.

Nielsen, L.J., Stuart, P., Pičmanová, M., Rasmussen, S., Olsen, C.E., Harholt, J., Møller, B.L. and Bjarnholt, N. (2016) Dhurrin metabolism in the developing grain of Sorghum bicolor (L.) Moench investigated by metabolite profiling and novel clustering analyses of time-resolved transcriptomic data. *BMC Genom.* **17**, 1021. https://doi.org/10.1186/s12864-016-3360-4.

Peiser, G.D., Wang, T.T., Hoffman, N.E., Yang, S.F., Liu, H.W. and Walsh, C.T. (1984) Formation of cyanide from carbon-1 of 1-aminocyclopropane-1-carboxylic acid during its conversion to ethylene. *PNAS*, **81**, 3059–3063.

Pičmanová, M., Neilson, E.H., Motawia, M.S. *et al.* (2015) A recycling pathway for cyanogenic glycosides evidenced by the comparative metabolic profiling in three cyanogenic plant species. *Biochem J.* **469**, 375–389.

Rahantaniaina, M.S., Li, S.C., Chatel-Innocenti, G., Tuzet, A., Issakidis-Bourguet, E., Mhamdi, A. and Noctor, G. (2017) Cytosolic and chloroplastic DHARs cooperate in oxidative stress-driven activation of the salicylic acid pathway. *Plant Physiol.* **174**, 956–971.

Rezaei, M.K., Shobbar, Z.S., Shahbazi, M., Abedini, R. and Zare, S. (2013) Glutathione S-transferase (GST) family in barley: Identification of members, enzyme activity, and gene expression pattern. *J. Plant Physiol.* **170**, 1277–1284.

Sanchez-Perez, R., Jørgensen, K., Olsen, C.E., Dicenta, F. and Møller, B.L. (2008) Bitterness in almonds. *Plant Physiol.* **146**, 1040–1052.

Seigler, D.S., Pauli, G.F., Frohlich, R., Wegelius, E., Nahrstedt, A., Glander, K.E. and Ebinger, J.E. (2005) Cyanogenic glycosides and menisdaurin from *Guazuma ulmifolia*, *Ostrya virginiana*, *Tiquilia plicata*, and *Tiquilia canescens*. *Phytochemistry*, **66**, 1567–1580.

Selmar, D., Irandoost, Z. and Wray, V. (1996) Dhurrin-6'-glucoside, a cyanogenic diglucoside from *Sorghum bicolor*. *Phytochemistry*, **43**, 569–572.

Siegien, I. and Bogatek, R. (2006) Cyanide action in plants - from toxic to regulatory. *Acta Physiol. Plant.* **28**, 483–497.

Simon, S. and Petrášek, J. (2011) Why plants need more than one type of auxin. *Plant Sci.* **180**, 454–460.

Su, T.B., Xu, J.A., Li, Y.A., Lei, L., Zhao, L., Yang, H.L., Feng, J.D., Liu, G.Q. and Ren, D.T. (2011) Glutathione-indole-3-acetonitrile is required for camalexin biosynthesis in *Arabidopsis thaliana*. *Plant Cell*, **23**, 364–380.

Swain, E. and Poulton, J.E. (1994) Utilization of amygdalin during seedling development of *Prunus serotina*. *Plant Physiol.* **106**, 437–445.

Tamura, K., Stecher, G., Peterson, D., Filipski, A. and Kumar, S. (2013) MEGA6: molecular evolutionary genetics analysis Version 6.0. *Mol. Biol. Evol.* **30**, 2725–2729.

Tocheva, E.I., Fortin, P.D., Eltis, L.D. and Murphy, M.E.P. (2006) Structures of ternary complexes of BphK, a bacterial glutathione S-transferase that reductively dechlorinates polychlorinated biphenyl metabolites. *J. Biol. Chem.* **281**, 30933–30940.

Urano, J., Nakagawa, T., Maki, Y., Masumura, T., Tanaka, K., Murata, N. and Ushimaru, T. (2000) Molecular cloning and characterization of a rice dehydroascorbate reductase. *FEBS Lett.* **466**, 107–111.

Winterberg, B., Du Fall, L.A., Song, X.M., Pascovici, D., Care, N., Molloy, M., Ohms, S. and Solomon, P.S. (2014) The necrotrophic effector protein SnTox3 re-programs metabolism and elicits a strong defence response in susceptible wheat leaves. *BMC Plant Biol.* **14**, 215. https://doi.org/10.1186/s12870-014-0215-5.

Xie, C., Zhong, D. and Chen, X. (2013) A fragmentation-based method for the differentiation of glutathione conjugates by high-resolution mass spectrometry with electrospray ionization. *Anal. Chim. Acta*, **788**, 89–98.

Xun, L.Y., Belchik, S.M., Xun, R., Huang, Y., Zhou, H.N., Sanchez, E., Kang, C. and Board, P.G. (2010) S-Glutathionyl-(chloro)hydroquinone reductases: a novel class of glutathione transferases. *Biochem J.* **428**, 419–427.

Zagrobelny, M., Bak, S. and Møller, B.L. (2008) Cyanogenesis in plants and arthropods. *Phytochemistry*, **69**, 1457–1468.